BEYOND-EXPERT PERFORMANCE WITH LIMITED DEMONSTRATIONS: EFFICIENT IMITATION LEARNING WITH DOUBLE EXPLORATION

Anonymous authors
Paper under double-blind review

ABSTRACT

Imitation learning is a central problem in reinforcement learning where the goal is to learn a policy that mimics the expert's behavior. In practice, it is often challenging to learn the expert policy from a limited number of demonstrations accurately due to the complexity of the state space. Moreover, it is essential to explore the environment and collect data to achieve beyond-expert performance. To overcome these challenges, we propose a novel imitation learning algorithm namely Imitation Learning with Double Exploration (ILDE), which implements exploration in two aspects: (1) optimistic policy optimization via an exploration bonus that rewards state-action pairs with high uncertainty to potentially improve the convergence to the expert policy, and (2) curiosity-driven exploration of the states that deviate from the demonstration trajectories to potentially yield beyond-expert performance. Empirically, we demonstrate that ILDE outperforms the state-of-the-art imitation learning algorithms in terms of sample efficiency and achieves beyond-expert performance on Atari and MuJoCo tasks with fewer demonstrations than those in previous work. We also provide theoretical justification of ILDE as an uncertainty-regularized policy optimization method with optimistic exploration, leading to a regret growing sublinearly in the number of episodes.

1 INTRODUCTION

Imitation learning (IL) is an important subfield of reinforcement learning (RL), in which ground truth rewards are not available and the goal is to learn a policy based on expert demonstrations. Often such demonstrations are limited, making it challenging to achieve expert-level performance. In practice, imitation learning is widely used in various applications such as autonomous vehicle navigation (Codevilla et al., 2018), robotic control (Finn et al., 2016; Zhang et al., 2018) and surgical assistance (Osa et al., 2014; Li et al., 2022).

As one of the simplest approaches of imitation learning, behavior cloning (Pomerleau, 1988) learns a policy directly from the state-action pairs in the demonstration dataset. More recent approaches to imitation learning, such as generative adversarial imitation learning (GAIL) (Ho & Ermon, 2016), use a discriminator to guide policy learning rather than directly learning a reward function based on demonstration trajectories. Due to matching occupancy based on a limited set of trajectories, it is still difficult for such algorithms to achieve better-than-expert performance and solve high-dimensional problems with limited demonstration data. Moreover, these techniques are typically unstable since the reward function is continually changing as the reward function is updated during the RL training. Alternative approaches, based on the curiosity (Yu et al., 2020; Pathak et al., 2017; Burda et al., 2018), a form of self-supervised exploration, encourage the agent to explore transitions that are distinct from the expert – thereby potentially yielding beyond-expert performance. Another benefit of the approach is related to the GIRIL algorithm specifically; that is, it uses a pre-trained auto-encoder, which makes the technique more stable (Yu et al., 2020).

As illustrated in Table 4 in Appendix A, this work seeks to formulate a sample-efficient imitation learning algorithm that combines the best of both worlds. That is, we integrate the stability and self-supervised exploration properties of GIRIL into discriminator-based imitation learning approaches.

Additionally improving the sample-efficiency with an exploration-bonus, we formulate the framework of Imitation Learning with Double Exploration (ILDE).

In detail, ILDE learns a policy based on an uncertainty-regularized discrepancy. The uncertainty-regularized discrepancy combines the distance to the expert policy, the cumulative uncertainty of the policy during exploration, and the cumulative uncertainty of the policy with respect to the demonstration dataset. To optimize the uncertainty-regularized discrepancy, ILDE utilizes a GAIL-based imitation reward while integrating two distinct forms of exploration. Firstly, through optimistic policy optimization, augmented by an exploration bonus, ILDE incentivizes the exploration of state-action pairs characterized by high uncertainty, thereby facilitating the training of the discriminator network, which functions as the reward model. Secondly, leveraging curiosity-driven exploration, ILDE targets transitions deviating from demonstration trajectories, paving the way for nuanced policy improvements.

The key contributions of this paper are summarized as follows:

- In Section 3, we theoretically formulate the problem of solving the aforementioned policy which minimizes the uncertainty-regularized discrepancy between the learner trajectories and demonstration trajectories.
- In Section 4, we present our proposed Algorithm ILDE with natural policy gradient (ILDE-NPG). we are then able to demonstrate the regret guarantee of ILDE-NPG in Theorem 4.7, which is the first theoretical guarantee for imitation learning in MDPs with nonlinear function approximation.
- Although ILDE-NPG is computationally intensive, we offer a more flexible version of ILDE in Section 5, focusing on two key exploration strategies: (1) encouraging the learner to explore state-action pairs that are 'far' from the current rollout dataset, and (2) rewarding benign deviations from the demonstration dataset using curiosity-based intrinsic rewards. We also demonstrate how to efficiently implement ILDE in practice.
- In Section 6, we present experimental results for a practical implementation of ILDE. Our findings demonstrate that ILDE surpasses existing baselines in terms of both average return and sample complexity. This underscores the practical advantages of our proposed objective for imitation learning.

2 Related Work

Imitation learning with limited demonstrations for beyond-expert performance. Learning from limited demonstrations in a high-dimensional environment is challenging, and the effectiveness of imitation learning methods is hampered (Li et al., 2024). Inverse reinforcement learning (IRL) methods (Ziebart et al., 2008; 2010; Boularias et al., 2011) seek a reward function that best explains the demonstration data, which makes it hard for them to achieve better-than-expert performance when the data is extremely limited. GAIL achieves impressive performance in low-dimensional environments via adversarial learning-based distribution matching. Variational adversarial imitation learning (VAIL) improves GAIL by compressing the information flow with a variational discriminator bottleneck (Peng et al., 2019).

Unfortunately, GAIL and VAIL do not scale well in high-dimensional environments (Brown et al., 2019), and still require many episodes of demonstrations. Recent work has focused on reducing the number of required demonstration episodes to between 5 and 20 episodes using techniques such as MCTS-based RL (Yin et al., 2022), patch rewards (Liu et al., 2023), and applying demonstration augmentation and a prior policy baseline Li et al. (2022). Techniques based on curiosity-driven exploration, such as CDIL (Pathak et al., 2017) and GIRIL (Yu et al., 2020), potentially provide a more scalable approach to imitation learning. In particular, Yu et al. (2020) propose the GIRIL algorithm within a setting with only a so-called one-life demonstration, which is only a partial episode of an Atari game. The system demonstrates favourable performance on Atari games when compared to GAIL, VAIL, and CDIL. Such techniques with intrinsic motivation have the advantage of allowing beyond-expert performance but the disadvantage of potentially optimising an objective that is not implied by the demonstrations. Our proposed ILDE system seeks to use curiosity-driven exploration as one of two sources of exploration to supplement a traditional imitation learning objective.

Beyond reducing the sheer amount of demonstration data, the problem of varying optimality scores and the reliability of demonstrations has also garnered more attention recently. Confidence-Aware Imitation Learning (CAIL) extends adversarial inverse reinforcement learning with a bi-level optimisation technique to concurrently learn the policy along with confidence scores reflecting the optimality of the demonstrations (Zhang et al., 2021). The setting of imbalanced demonstrations has been studied from a semi-supervised learning perspective (Fu et al., 2023) as well as within multi-modal imitation learning (Gu & Zhu, 2024). We focus on an alternative approach to the problem of demonstration reliability which combines curiosity with a traditional imitation reward.

Reinforcement learning from demonstrations (RLfD). An alternative framework, related to imitation learning, is reinforcement learning from demonstrations (RLfD) (Hester et al., 2018; Christiano et al., 2017; Zhu et al., 2022). While potentially offering accelerated policy learning, such techniques require ground-truth rewards, which are not available in pure imitation learning settings.

Exploration bonuses and optimistic RL. Optimism is a long-standing principle in RL, where it typically refers to overestimating the value of a particular state or state-action pair in order to make the state or state-action pair known more rapidly through increased visitations – essentially, this implies unknown state-action pairs are given a large exploration bonus while known state-action pairs are given little to no exploration bonus. Analogous to upper confidence bound (UCB) bandit algorithms (Auer et al., 2002), various techniques have been implemented in RL which use confidence bounds to upper bound the value in a probabilistic sense. Such techniques traditionally use concentration inequalities based on visitation counts for each state-action pair, which gives such techniques a firm statistical grounding but which limits them to discrete state-action spaces (Shani et al., 2020; Fruit et al., 2018; Jaksch et al., 2010).

Recent techniques have aimed at making exploration bonuses more scalable. E3B provides an approximate approach to visitation counts by maintaining a covariance matrix which implicitly captures the relations between visited states (Henaff et al., 2023). State Entropy directly aims to maximise the entropy over the states, rewarding states in a batch according to the log of their distance to its k-nearest neighbour state (Seo et al., 2021).

Theoretical guarantees for imitation learning. There is a large body of literature on imitation learning for tabular MDPs (Cai et al., 2019; Chen et al., 2019; Zhang et al., 2020; Xu et al., 2020; Shani et al., 2022; Chang et al., 2021). Subsequently, Liu et al. (2021) studied imitation learning for linear kernel MDPs and provided an $\widetilde{O}(\sqrt{H^4 d^3 T})$ regret bound, where d is the dimension of the feature space, H is the horizon of the MDPs, T is the number of episodes. Viano et al. (2022) considered linear MDPs and proposed PPIL, which achieved a sample complexity of $O(d^2/(1-\gamma)^9\epsilon^5)$ in discounted linear MDPs. Our work considers MDPs with general function approximation, utilizing the generalized Eluder dimension (Agarwal et al., 2023; Zhao et al., 2023) to characterize the complexity of the function class.

3 PRELIMINARIES

We consider an episodic MDP $(\mathcal{S}, \mathcal{A}, H, \mathbb{P}, r)$, where $\mathcal{S}$ and $\mathcal{A}$ are the state and action spaces, respectively, H is the length of each episode, $\mathbb{P}_h$ is the Markov transition kernel of the h-th step of each episode for any $h \in [H]$, and $r : S \times A \to [-1, 1]$ is the reward function. We assume without loss of generality that the reward function r is deterministic.

In the episodic MDP, the agent interacts with the environment as follows. At the beginning of each episode $t \in [T]$, the agent chooses a policy $\pi^t = \{\pi_h^t\}_{h\in[H]} \in \Delta(\mathcal{A}|\mathcal{S}, H)$. Then the agent takes the action $a_h^t \sim \pi_h^t(\cdot|s_h^t)$ at the h-th step of the t-th episode and transits to the next state $s_{h+1}^t \sim \mathbb{P}_h(\cdot|s_h^t, a_h^t)$ without observing the reward. The episode terminates when the agent reaches the state s_{H+1}^t. Without loss of generality, we assume that the initial state $s_1 = x$ is fixed across different episodes. We remark that our algorithms and corresponding analyses readily generalize to the setting where the initial state s_1 is sampled from a fixed distribution.

We now define the value functions in the episodic MDP. For any policy $\pi = \{\pi_h\}_{h\in[H]}$ and reward function $r : \mathcal{S} \times \mathcal{A} \to [-1, 1]$, the state value function V and action-value function Q are defined for

any $(s, a, h) \in \mathcal{S} \times \mathcal{A} \times [H]$ as follows,

$$V^r_{h,\pi}(s) = \mathbb{E}_{\pi_h}\Big[\sum_{i=h}^{H} r(s_i, a_i) \mid s_h = s\Big], \;\; Q^r_{h,\pi}(s, a) = \mathbb{E}_{\pi_h}\Big[\sum_{i=h}^{H} r(s_i, a_i) \mid s_h = s, a_h = a\Big], \tag{3.1}$$

where the expectation $\mathbb{E}_\pi[\cdot]$ is taken with respect to the action $a_i \sim \pi_i(\cdot|s_i)$ and the state $s_{i+1} \sim \mathbb{P}_i(\cdot|s_i, a_i)$ for any $i \in \{h, h+1, \ldots, H\}$. With slight abuse of notations, we also denote by $\mathbb{P}_h$ the operator form of the transition kernel such that $(\mathbb{P}_h f)(s, a) = \mathbb{E}_{s' \sim \mathbb{P}_h(\cdot|s,a)}[f(s')]$ for any $f : S \to \mathbb{R}$. By the definitions of the value functions in (3.1), for any $(s, a, h) \in S \times A \times [H]$, any policy π, and any reward function r, we have

$$V^r_{h,\pi}(s) = \langle Q^r_{h,\pi}(s, \cdot), \pi_h(\cdot, s)\rangle_A, \quad Q^r_{h,\pi}(s, a) = r_h(s, a) + \mathbb{P}_h V^r_{h+1,\pi}(s, a), \quad V^r_{H+1,\pi}(s) = 0, \tag{3.2}$$

where $\langle \cdot, \cdot \rangle_A$ denotes the inner product over the action space A. We further define the expected cumulative reward as follows,

$$J(\pi, r) = V^r_{1,\pi}(x).$$

We assume that there is an unknown expert policy $\pi^E = \{\pi^E_h\}_{h\in[H]} \in \Delta(\mathcal{A}|\mathcal{S}, H)$ that achieves a high expected cumulative reward $J(\pi^E, r^*)$ under the unknown underlying reward function r^*. Given n demonstration trajectories $\tau^E = \{(s^{(j)}_i, a^{(j)}_i)\}^H_{i=1}$ for $j \in [n]$, the goal of imitation learning is to learn a policy π that achieves a potentially high expected cumulative reward $J(\pi, r^*)$ under the unknown reward function r^* based on the expert demonstration. As introduced in Chen et al. (2019), we characterize the discrepancy between the expert policy π^E and the learner policy π by the following Integral Probability Metric (IPM) over the stationary distributions of the MDP.

Definition 3.1 (Definition 2, Chen et al. 2019)**.** Let $\mathcal{R}$ denote a class of symmetric reward functions $r : \mathcal{S} \times \mathcal{A} \to [-1, 1]$, i.e., if $r \in \mathcal{R}$, then $-r \in \mathcal{R}$. Given two policies $\pi, \pi' \in \Delta(\mathcal{A}|\mathcal{S}, H)$, the $\mathcal{R}$-distance is defined as

$$d_{\mathcal{R}}(\pi, \pi') = \sup_{r\in\mathcal{R}} \big|J(\pi^E, r) - J(\pi, r)\big|.$$

Remark 3.2. The IPM distance is a versatile tool for evaluating GAN models. In the context of imitation learning, we can choose different classes of reward functions $\mathcal{R}$ to measure the discrepancy between the expert policy and the learner policy. For instance, we can choose $\mathcal{R}$ to be the class of symmetric reward functions that are 1-Lipschitz continuous with respect to the state-action pair (s, a), which corresponds to the Wasserstein distance. Or we can choose $\mathcal{R}$ to be the unit ball in an RKHS, which yields kernel maximum mean discrepancy (MMD).

As proposed in Yu et al. (2020), to encourage the agent to explore the environment and learn a beyond-expert policy, it is essential to incorporate *uncertainty-driven* (intrinsic-reward-driven) exploration into the imitation learning framework. In contrast to GIRIL (Yu et al., 2020) which purely relies on the intrinsic reward to explore transitions that are distinct from the expert demonstration, we consider learning a policy which mimics the expert policy subject to an intrinsic reward regularisation term. To this end, we defined the following objective function:

$$\min_{\pi\in\Delta(\mathcal{S}|\mathcal{A},H)} \max_{r\in\mathbb{R}} \big(J(\pi^E, r) - J(\pi, r) - \lambda \cdot \mathrm{Int}(\pi; \tau^E)\big), \tag{3.3}$$

where $\mathrm{Int}(\pi; \tau^E)$ is the expected cumulative intrinsic reward of the policy π under the expert demonstration τ^E. More specifically,

$$\mathrm{Int}(\pi; \tau^E) := \mathbb{E}_{\pi, \widehat{s}_{h+1}\sim\widehat{\mathbb{P}}(\cdot|s_h,a_h)}\Big[\sum_{h=1}^{H} \mathcal{L}(\widehat{s}_{h+1}, s_{h+1})\Big],$$

where $\widehat{\mathbb{P}}$ is the estimated transition probability that is estimated as follows:

$$\widehat{\mathbb{P}} := \operatorname*{argmin}_{\mathbb{P}\in\mathcal{P}^{model}} \sum_{j=1}^{n}\sum_{i=1}^{H} \mathbb{E}_{\widehat{s}_{i+1}\sim\mathbb{P}(\cdot|s^{(j)}_i, a^{(j)}_i)}\Big[\mathcal{L}(\widehat{s}_{i+1}, s^{(j)}_{i+1})\Big]$$

is a trained transition model over the demonstration trajectories τ^E, and $\mathcal{L}$ is a distance metric (e.g. $\mathcal{L}(\widehat{s}_{i+1}, s_{i+1}^{(j)}) = ||\widehat{s}_{i+1} - s_{i+1}^{(j)}||_2^2$). (Empirically, it is the trained VAE model which samples the next state as proposed in Yu et al. (2020) and Pathak et al. (2017).) For simplicity, we denote the intrinsic reward as the following form

$$\mathcal{L}_{\tau^E,h}(s,a) = \mathbb{E}_{\widehat{s}' \sim \widehat{\mathbb{P}}_h(\cdot|s,a), s' \sim \mathbb{P}_h(\cdot|s,a)} \big[\mathcal{L}(\widehat{s}', s')\big]. \tag{3.4}$$

As a shorthand, we define **uncertainty-regularized loss function** for a policy π and a reward function r as follows,

$$\ell(\pi, r) = J(\pi^E, r) - J(\pi, r) - \lambda \cdot \text{Int}(\pi; \tau^E). \tag{3.5}$$

Imitation Learning. As shown in (3.3) and (3.5), our goal is to learn an optimal policy π^* which minimizes the following worst-case loss:

$$\pi^* = \operatorname*{argmin}_{\pi \in \Delta(\mathcal{A}|\mathcal{S},H)} \max_{r \in \mathbb{R}} \ell(\pi, r). \tag{3.6}$$

Conjecture. To achieve the optimal policy as defined in (3.6), we hypothesize that a more principled exploration technique is needed to adapt to the dynamic rewards during the training process. Additionally, we conjecture that such uncertainty regularization will help the learner attain performance beyond the expert level.

In the previous theoretical formulation of online imitation learning (Chen et al., 2019; Liu et al., 2021), the objective is to learn a policy which is close to the expert policy with respect to the $\mathcal{R}$-distance. Thus, the optimal policy under their formulation is π^E and the loss at the saddle point is zero. By contrast, our optimal policy π^* is non-trivially different from the expert policy π^E.

In this work, we aim to find π^* by proposing a novel theory-guided policy optimization algorithm with uncertainty-aware exploration.

Under the online learning setting, we define the uncertainty regularized regret as follows:

$$\text{Regret}(T) = \max_{r \in R} \sum_{t=1}^{T} \ell(\pi^t, r) - \ell(\pi^*, r).$$

To achieve the objective (3.3) under the online learning regime, we aim for designing an imitation learning algorithm to achieve a Regret(T) growing sublinear as a function of T. Then we can show that $\mathbb{E}[\ell(\pi_{out}, r)]$ converges to $\ell(\pi^*, r)$ as $T \to \infty$ for any $r \in \mathbb{R}$, where π_{out} refers to the hybrid policy sampled uniformly from $\{\pi^t\}_{t \in [T]}$.

4 Imitation Learning with Double Exploration (ILDE)

We now turn to introducing the ILDE framework theoretically before its implementation in Section 5. We analyze ILDE using mirror descent as the policy optimization technique which is more amenable to theoretical analysis than scalable techniques such as PPO. The theoretical analysis considers a general data collection subroutine of which on-policy data collection used in the practical implementation is a special case. The theoretical analysis further considers an IPM-based GAN and a bonus based on state-action uncertainty as proposed by (Agarwal et al., 2023). In practice, we apply GAIL and state entropy (Seo et al., 2021). Since PPO already applies action entropy in the policy optimisation, together the state entropy and action entropy help to explore unvisited state action pairs in similar manner.

4.1 Algorithm

This subsection instantiates a theoretical version of ILDE, where we apply Optimistic Natural Policy Gradient (Liu et al., 2024) as a policy optimization module. Since Algorithm 1 is a phasic policy optimization algorithm, the number of episodes where the learner interacts with the environment is indeed $T = K \cdot N/m$.

Imitation reward Module. In Line 4 of Algorithm 1, the learner samples a data set with N trajectories. With a carefully chosen N, the expected uncertainty of each state-action pair $(s, a) \in$

Algorithm 1 ILDE with Natural Policy Gradient

1: **input**: number of iterations K, period of collecting fresh data m, batch size N, learning rate η, demonstration trajectories τ^E, reward function r^1, loss function $\mathcal{L}_{\tau^E}$.
2: **initialize:** for all $(h, s) \in [H] \times \mathcal{S}$ set $\pi_h^1(\cdot \mid s) = \text{Uniform}(\mathcal{A})$
3: **for** $k = 1, \ldots, K$ **do**
4: **if** $k \bmod m = 1$ **then**
5: $\mathcal{D}^k \leftarrow \{N$ fresh trajectories $\overset{\text{i.i.d.}}{\sim} \pi^{k'}\}$, where k' is chosen uniformly at random from $\{\max(1, k-m+1), \ldots, k-1, k\}$.
6: **else**
7: $\mathcal{D}^k \leftarrow \mathcal{D}^{k-1}$.
8: $r^k \leftarrow r^{k-1}$.
9: **end if**
10: Update r^k by projected gradient descent with estimated $-L(\pi^k, r^k)$.
11: $\{Q_h^k\}_{h\in[H]} \leftarrow \text{OPE}(\pi^k, \mathcal{D}^k, r^k, \mathcal{L}_{\tau^E})$.
12: for all $(h, s) \in [H] \times \mathcal{S}$ update $\pi_h^{k+1}(\cdot \mid s) \propto \pi_h^k(\cdot \mid s) \cdot \exp(\eta \cdot Q_h^k(s, \cdot))$
13: **end for**
14: **output**: π_{out} that is sampled uniformly at random from $\{\pi^k\}_{k\in[K]}$.

Algorithm 2 $\text{OPE}(\pi, \mathcal{D}, r, \mathcal{L}_{\tau^E})$

Split $\mathcal{D}$ evenly into H disjoint sets $\mathcal{D}_h$ for $h \in [H]$.
Set $V_{H+1}(s) \leftarrow 0$ for all $s \in \mathcal{S}$
for $h = H, \cdots, 1$ **do**
 $\widehat{f}_h \leftarrow \text{argmin}_{f_h \in \mathcal{F}_h} \sum_{(s_h, a_h)\in\mathcal{D}_h} (f_h(s_h, a_h) - V_{h+1}(s_{h+1}))^2$.
 for $(s, a) \in \mathcal{S} \times \mathcal{A}$ **do**
 Compute exploration bonus $b_h(s, a)$ as in (4.4).
 $Q_h(s, a) \leftarrow \text{clip}_{[-H,H]}\big(\widehat{f}_h(s, a) + \widetilde{r}_h(s, a) + b_h(s, a)\big)$,
 where $\widetilde{r}_h(s, a) \leftarrow r(s, a) + \lambda \mathcal{L}_{\tau^E,h}(s, a)$.
 $V_h(s) \leftarrow \mathbb{E}_{a\sim\pi_h(\cdot|s)} [Q_h(s, a)]$.
 end for
end for
output $\{Q_h\}_{h=1}^H$

$\mathcal{S} \times \mathcal{A}$ is upper bounded by $\widetilde{O}(1/\sqrt{N})$, where we omit the dependency of H and generalized Eluder dimension.

After updating the on-policy dataset, in Line 10, the agent can optimize the reward function according to the following loss function:

$$L(\pi, r) = J(\pi^E, r) - J(\pi, r). \tag{4.1}$$

While L is unknown for the learner, in Line 10 of Algorithm 1, we compute an empirical estimate of L:

$$\widehat{L}(\pi^k, r) = \frac{1}{n} \cdot \sum_{j=1}^{n} \sum_{h=1}^{H} r(s_h^{(j)}, a_h^{(j)}) - \frac{1}{N} \cdot \left[\prod_{h=1}^{H} \frac{\pi_h^k(a_h \mid s_h)}{\pi_h^{t_k}(a_h \mid s_h)}\right] \cdot \sum_{\tau\in\mathcal{D}^k} \sum_{h=1}^{H} r(s_h^{(\tau)}, a_h^{(\tau)}), \tag{4.2}$$

where t_k is the index of the last policy which is used to collect fresh data at iteration k.

Assumption 4.1 (Convexity and Lipschitz Continuity of the reward function)**.** We assume that the reward function r is parameterized by a set of parameters $\boldsymbol{\theta} \in \Theta \subset \mathbb{R}^d$ and the estimated loss function $\widehat{L}$ is convex with respect to $\boldsymbol{\theta}$. For any $\boldsymbol{\theta}_1, \boldsymbol{\theta}_2 \in \Theta$, $\|\boldsymbol{\theta}_1 - \boldsymbol{\theta}_2\|_2 = O(1)$, and for any $\boldsymbol{\theta} \in \Theta$, $s, a \in \mathcal{S} \times \mathcal{A}$, $\|\nabla_{\boldsymbol{\theta}} r_{\boldsymbol{\theta}}(s, a)\|_2 = O(1)$.

As a result, in Line 10, we essentially update the reward function r^k by the following projected gradient descent:

$$\boldsymbol{\theta}^{k+1} = \text{proj}_{\Theta}\big(\boldsymbol{\theta}^k - \eta_{\boldsymbol{\theta}} \cdot \nabla_{\boldsymbol{\theta}}[-\widehat{L}(\pi^k, r^k)]\big). \tag{4.3}$$

To ensure that $\widehat{L}$ is reflecting L accurately, we also require the following assumption on the quality of the demonstration trajectories.

Assumption 4.2 (Quality of the demonstration trajectories)**.** We assume that the demonstration trajectories τ^E satisfies the following property for any reward function $r \in \mathcal{R}$:

$$\left| \frac{1}{n} \sum_{j=1}^{n} \sum_{h=1}^{H} r(s_h^{(j)}, a_h^{(j)}) - J(\pi^E, r) \right| \leq \epsilon_E$$

for some $\epsilon_E > 0$.

Policy optimization module. The algorithm is a phasic policy optimization algorithm built upon Liu et al. (2024). In Line 12, the policy π_h^{k+1} is obtained by taking a mirror descent step from π_h^k, maximizing the following KL-regularized return-value estimation:

$$\pi_h^{k+1} = \arg\min_{\pi_h} \eta \cdot \sum_s \pi_h(s) \cdot \langle Q_h^k(s, \cdot), \pi_h(s) \rangle + d_{KL}(\pi_h | \pi_h^k).$$

where Q_h^k is computed by an optimistic policy evaluation (OPE) subroutine to guide the direction of policy updating.

Double Exploration in Algorithm 2. While widely-used algorithms in empirical studies, such as PPO, directly use empirical returns to guide the policy updating procedure, we employ Algorithm 2 to estimate the expected return from all state-action pairs.

In OPE (Algorithm 2), we set an exploration bonus according to Lemma C.3,

$$b_h(s, a) = \sqrt{8H^2 \log(H \cdot \mathcal{N}_{\mathcal{F}}(\epsilon_{\mathcal{F}})/\delta) + 4\epsilon_{\mathcal{F}} N + \gamma} \cdot D_{\mathcal{F}_h}((s, a); \mathcal{D}_h), \tag{4.4}$$

where $D_{\mathcal{F}_h}$ is defined in Definition 4.3 as an exploration bonus to encourage the policy to explore the state-action pairs whose expected return values are hard to predict given the on-policy dataset $\mathcal{D}^k$.

Additionally, we utilize a pretrained uncertainty evaluation function $\mathcal{L}_{\tau^E}$ to explore states beyond the demonstration trajectories. Then, in lines 3-10, we use value iteration to compute the value function considering the sum of the imitation reward r^k, the exploration bonus b_h^k, and the uncertainty $\mathcal{L}$.

4.2 Theoretical Analysis

With the ILDE framework introduced in Section 4, we provide a thorough regret analysis for Algorithm 1.

Our analysis addresses a broad category of MDPs, specifically those whose value functions can be effectively approximated and generalized across various state-action pairs. These are referred to as MDPs with bounded generalized Eluder dimension (Agarwal et al., 2023).

Definition 4.3 (Generalized Eluder dimension, Agarwal et al. 2023)**.** Let $\lambda_{\text{ED}} \geq 0$, a sequence of state-action pairs $\mathbf{Z} = \{z_i\}_{i \in [T]} \in (\mathcal{S}, \mathcal{A})^{\otimes T}$. The generalized Eluder dimension of a value function class $\mathcal{F} : \mathcal{S} \times \mathcal{A} \to [-H, H]$ with respect to λ_{ED} is defined by $\dim_T(\mathcal{F}) := \sup_{\mathbf{Z}:|\mathbf{Z}|=T} \dim(\mathcal{F}, \mathbf{Z})$,

$$\dim(\mathcal{F}, \mathbf{Z}) := \sum_{i=1}^{T} \min\left(1, D_{\mathcal{F}}^2(z_i; z_{[i-1]})\right),$$

$$\text{where } D_{\mathcal{F}}^2(z; z_{[t-1]}) := \sup_{f_1, f_2 \in \mathcal{F}} \frac{(f_1(z) - f_2(z))^2}{\sum_{s \in [t-1]} (f_1(z_s) - f_2(z_s))^2 + \lambda_{\text{ED}}}.$$

We write $\dim_T(\mathcal{F}) := H^{-1} \cdot \sum_{h \in [H]} \dim_T(\mathcal{F}_h)$ for short when $\mathcal{F}$ is a collection of function classes $\mathcal{F} = \{\mathcal{F}_h\}_{h=1}^H$ in the context.

Remark 4.4. The concept of generalized Eluder dimension was first introduced in Agarwal et al. (2023), where a value-based algorithm was proposed to achieve a nearly optimal regret bound in the online RL setting. Notably, our definition of the function class is somewhat broader, as we apply an unweighted definition of the $D_{\mathcal{F}}$ distance. Consequently, the definition of generalized Eluder dimension does not require taking the supremum over weights, allowing for a wider class of MDPs.

The analyzed policy optimization method needs a policy evaluation subroutine as introduced in Algorithm 2. To make such a policy evaluation tractable, we make the following realizability assumption.

Assumption 4.5 (Strong realizability of state-action value function class)**.** For all $h \in H$ and $V_{h+1} : \mathcal{S} \to [-H, H]$, there exists a function $f_h \in \mathcal{F}_h$ such that for all $s \in \mathcal{S}$, $a \in \mathcal{A}$, we have $f_h(s,a) = \mathbb{P}_h V_{h+1}(s,a)$.

Definition 4.6 (Covering numbers of function classes)**.** For each $h \in [H]$, there exists an $\epsilon_{\mathcal{F}}$-cover $\mathcal{C}(\mathcal{F}_h, \epsilon_{\mathcal{F}}) \subseteq \mathcal{F}_h$ with size $|\mathcal{C}(\mathcal{F}_h, \epsilon_{\mathcal{F}})| \leq \mathcal{N}(\mathcal{F}_h, \epsilon_{\mathcal{F}})$, such that for any $f \in \mathcal{F}$, there exists $f' \in \mathcal{C}(\mathcal{F}_h, \epsilon_{\mathcal{F}})$, such that $\|f - f'\|_\infty \leq \epsilon_{\mathcal{F}}$. For any $\epsilon_{\mathcal{F}} > 0$, we define the uniform covering number of $\mathcal{F}$ with respect to $\epsilon_{\mathcal{F}}$ as $\mathcal{N}_{\mathcal{F}}(\epsilon_{\mathcal{F}}) := \max_{h \in [H]} \mathcal{N}(\mathcal{F}_h, \epsilon_{\mathcal{F}})$.

Theorem 4.7 (Regret bound for Algorithm 1)**.** Suppose Assumptions 4.5, 4.1 and 4.2 hold. if we set $\gamma = H^2$, $\epsilon_{\mathcal{F}} = 1/N$, $\eta = \sqrt{\log|\mathcal{A}|}/H\sqrt{K}$, $m = \sqrt{K}/H\sqrt{\log|\mathcal{A}|}$, $\eta_{\boldsymbol{\theta}} = O(1/\sqrt{H^2 K})$, and $N = KH \dim_T(\mathcal{F}) \log \mathcal{N}_{\epsilon_{\mathcal{F}}}(\mathcal{F}) / \sqrt{\log|\mathcal{A}|}$, where $K = \left(\frac{T}{H^2 \dim_T(\mathcal{F}) \log \mathcal{N}_{\epsilon_{\mathcal{F}}}(\mathcal{F})}\right)^{2/3}$, then with probability at least $1 - \delta$, Algorithm 1 yields a regret of

$$\widetilde{O}\left(H^{8/3}\big(\dim_T(\mathcal{F}) \log \mathcal{N}_{\epsilon_{\mathcal{F}}}(\mathcal{F})\big)^{1/3} T^{2/3} + \epsilon_E T\right). \tag{4.5}$$

Remark 4.8. This is the first theoretical guarantee for imitation learning in MDPs with nonlinear function approximation. As shown in Zhao et al. (2023), the considered setting captures MDPs with bounded Eluder dimension (Russo & Van Roy, 2013) and thus also captures linear MDPs (Jin et al., 2020) as special cases. If we select a policy from $\{\pi^k\}_{k=1}^K$ uniformly at random, the expected loss for that policy is $O(\epsilon + \epsilon_E)$ when $T = \widetilde{\Theta}(H^8 \dim_T(\mathcal{F}) \log \mathcal{N}_{\epsilon_{\mathcal{F}}}(\mathcal{F})/\epsilon^3)$, which provides a sample complexity bound for Algorthm 1.

5 Practical Implementation of ILDE

Algorithm 3 Imitation Learning with Double Exploration (ILDE)

1: **input**: number of episodes T, period of collecting fresh data m, batch size N, learning rate η, demonstration trajectories τ^E, reward function r^1, pretrained loss function $\mathcal{L}_{\tau_E}$.
2: **for** $t = 1, \ldots, T$ **do**
3: Sample trajectories $\mathcal{D}^t$ from π^t.
4: Update the imitation reward r^t by minimizing the loss of the discriminator trained to distinguish between the demonstration trajectories and $\mathcal{D}^t$ (e.g. (5.1)).
5: Compute the aggregated reward $\widetilde{r}^t(s,a) = r^t(s,a) + \lambda \mathcal{L}_{\tau_E}(s,a)$ for all state-action pairs (s,a) in $\mathcal{D}^t$.
6: Update the current policy π^t via policy optimization method (e.g., PPO) with reward $\widetilde{r}^t(s,a) + b(s,a)$ where $b(s,a)$ is the exploration bonus and obtain π^{t+1}.
7: **end for**

While Algorithm 1 provides a solid sample-complexity guarantee, it lacks computational efficiency and is challenging to implement at scale. In this section, we concentrate on the crucial elements of Algorithm 1 and introduce the proposed Imitation Learning with Double Exploration (ILDE) framework. The algorithm, summarized in pseudocode in Algorithm 3, includes the following key modules:

- Imitation reward module: This module minimises the loss of a discriminator which distinguishes between demonstration data τ^E and data obtained during policy optimisation $\mathcal{D}^t$. Theoretically, the imitation reward function is progressively optimized according to the gap between the average return of demonstration trajectories and that of current trajectories. In practice, to implement the module, we maintain a discriminator D_θ which continue minimizing the following loss:

$$\mathbb{E}_{(s,a)\sim\tau^E}\big[\log D_\theta(s,a)\big] + \mathbb{E}_{(s,a)\sim\pi^t}\big[\log(1 - D_\theta(s,a))\big] + \beta \mathbb{E}_{s\sim\pi^t}\big[d_{KL}(E'(z|s)|r^t) - I_c\big], \tag{5.1}$$

  where encoder E' is introduced to incorporate a variational discriminator bottleneck (Peng et al., 2019) to improve GAIL, β is the scaling weight, and I_c is the information constraint.
- Pretrained uncertainty evaluation module: To implement this module, we make use of GIRIL. That is, we pretrain a VAE model to estimate the transition kernel $\widehat{\mathbb{P}}$ over the demonstration trajectories τ^E and compute the intrinsic reward $\mathcal{L}_{\tau^E,h}(s,a)$ (3.4) for all (s,a) in $\mathcal{D}^t$.
- Exploration bonus b: The exploration bonus provides an additional reward for state-action pairs with high uncertainty, thereby encouraging the agent to make estimated quantities relation to

such state-action pairs known with greater certainty, i.e. by visiting them more frequently. To analyze the ILDE framework theoretically in Section 4, we choose the $D_{\mathcal{F}}$-uncertainty of state-action pairs as the exploration bonus, which reflects the uncertainty of a state-action pair after collecting enough data using the current policy. To efficiently implement the exploration bonus in practice, we utilize state entropy (Seo et al., 2021) in a representation space of a feature extractor f. We utilize a k-nearest neighbor entropy estimator to calculate the exploration bonus as $b(s, a) = \log(||y - y^{k-\text{NN}}||_2 + 1)$, where $y = f(s)$ is a state representation from f and $y^{k-\text{NN}}$ is the k-nearest neighbor of y within a set of N representations $\{y_1, y_2, \cdots, y_N\}$, where N is the batch size. The state-dependency rather than state-action dependency of the bonus is motivated by the technique of entropy regularisation in the policy optimisation, which encourages spread across the action space particularly when there is high uncertainty over the optimal action.

- Policy optimisation module: While the above modules provide the design of the reward, the policy optimisation module optimises the policy for the objective. For policy optimisation, we use an actor-critic variant of proximal policy optimization (PPO) (Schulman et al., 2017) with generalized advantage updating.

6 EXPERIMENTS

We now conduct experiments based on four key hypotheses. First, we hypothesise that pure imitation learning methods such as VAIL will fail with limited demonstrations. Second, we hypothesise that a pre-trained model-based exploration reward such as GIRIL alone provides a stable improvement but may not reach a wide set of states due to the curiosity bias preferring certain states. Third, the state entropy reward bonus provides an exploration reward which provides a high reachability across a wide variety of states, thereby improving sample efficiency and overall performance. Fourth, VAIL's imitation reward can provide additional performance gains compared to pure exploration (i.e. exploration bonus and/or curiosity reward) when the imitation reward is reliable while there is no effect when the imitation reward is unreliable.

6.1 ATARI GAMES

To test these hypotheses, we compare our proposed ILDE to VAIL, GIRIL, and ablations on six Atari games within OpenAI Gym (Brockman et al., 2016) in a challenging setting where the agent receives even less demonstration data than in so-called one-life demonstration data (Yu et al., 2020). The imitation learning agents are trained according to the design of the imitation reward and/or any potential bonuses but are evaluated based on their actual scores on the Atari games. We summarize more experimental details in the Appendix B.

Demonstrations. A one-life demonstration only contains the states and actions performed by an expert player until they die for the first time in a game. We generate the one-life demonstrations using a PPO agent trained with ground-truth rewards for 10 million simulation steps. Table 5 in the Appendix B.1 shows that a one-life demonstration contains much less data than a full-episode demonstration. To make the problem even more challenging than prior work, the imitation learning agents receive demonstrations which comprise only 10% of a full one-life demonstration.

Baselines. We compare our ILDE with the following baselines: (1) VAIL (Peng et al., 2019), an improved GAIL variant using variation discriminator bottleneck, which updates the policy based on r^k only; (2) GIRIL (Yu et al., 2020), the generative intrinsic reward-driven imitation learning method; (3) ILDE w/o b, an ablation of ILDE without the exploration bonus b; and (4) ILDE w/o r^k, an ablation of IDLE without the imitation reward r^k.

Results. Table 1 compares the performance of our ILDE and other baselines. ILDE outperforms the other baselines in terms of achieving higher average returns and outperforming experts in more games. Notably, ILDE achieves an average performance that is 5.33 times of the expert demonstrator across the 6 Atari games. More specifically, ILDE outperforms the expert in all of the 6 Atari games and outperforms GIRIL in 4 games. The ablation study in Table 1 indicates the significance of each reward component.

Table 2 compares the sample efficiency of ILDE and other baselines. The results are the minimal steps after which imitation learning methods continuously outperform the experts until the end (50 million

Table 1: Average return of Expert demonstrator, VAIL, GIRIL, ILDE w/o $\lambda\mathcal{L}_{\tau_E}$, ILDE w/o b, ILDE w/o r^k and ILDE with one-life demonstration data on six Atari games. The results are reported in the format of $\text{mean} \pm \text{std}$ over 10 random seeds with better-than-GIRIL performance in bold. "#Games>Expert" denotes the number and ratio of games that an imitation learning method outperforms the expert. "Improve vs Expert" denotes the average performance improvements of IL methods versus the expert across 6 Atari games.

Atari Games	Expert	VAIL (r^k)	GIRIL	ILDE w/o $\lambda\mathcal{L}_{\tau_E}$	ILDE w/o b	ILDE w/o r^k	ILDE
BeamRider	1,918±645	91±116	8,524±1,085	3,233±3,340	8,521±1,234	**11,453±2,416**	**11,453±2,319**
DemonAttack	8,820±2,893	979±863	72,381±19,851	143±120	**78,513±11,553**	60,931±10,376	64,498±13,294
BattleZone	22,410±5,839	5,081±4,971	25,203±22,868	5,412±1,816	18,179±21,181	**43,708±22,733**	**59,109±25,575**
Qbert	6,246±2,964	3,754±4,460	76,491±81,265	10,849±5,018	26,900±52,146	54,169±68,305	70,566±75,310
Krull	6,520±941	7,937±8,183	20,935±23,796	857±916	16,715±23,153	**27,495±28,773**	**23,716±16,790**
StarGunner	22,495±11,516	219±182	542±188	764±455	478±239	**16,526±32,946**	**25,361±38,557**
#Games>Expert	0 / 0%	1 / 16.7%	5 / 83.3%	2 / 33.3%	4 / 66.7%	5 / 83.3%	**6 / 100%**
Improve vs Expert	1.0	0.37	4.87	0.64	3.50	4.71	**5.33**

Table 2: Sample efficiency improvements averaged over 6 games.

Sample Efficiency	VAIL (r^k)	GIRIL	ILDE w/o b	ILDE w/o r^k	ILDE
Improve vs GIRIL	-418.32%	0%	-14.05%	24.92%	22.68%

steps). To quantitatively compare the sample efficiency improvements of ILDEs versus GIRIL, we regard the results indicated by '-' as 100%, and calculate the improvement ratios on sample efficiency. "Improve vs GIRIL" presents the average sample efficiency improvements over 6 Atari games. ILDE archives much higher sample efficiency improvements than GIRIL. More details can be found in Table 10 and 11 of Appendix B.2.5.

6.2 Continuous control tasks

Additionally, we also conduct experiments on the MuJoCo environments. Table 3 compares the performance of ILDE and other baselines. ILDE consistently outperforms other baselines in the four continuous control tasks by achieving higher average returns over 10 random seeds. We summarized more experimental details for MuJoCo experiments in Appendix B.2.6. Based on our current experiments, we observed that ILDE performs exceptionally well in games, while its improvement on MuJoCo is less significant. This may suggest that the current design of the intrinsic reward is better suited for tasks with human-designed rewards.

Table 3: Average return of VAIL, GIRIL, and ILDE on the MuJoCo tasks. The average returns are calculated on the last 4 evaluation points. The results are reported in the format of $\text{mean} \pm \text{std}$ over 10 random seeds with the best performance in bold.

Tasks	VAIL (r^k)	GIRIL	ILDE
Reacher	-499±183	-60±24	**-51±15**
Hopper	1,264±783	1,447±273	**1,878±690**
Walker2d	879±825	997±575	**998±694**
HumanoidStandup	52,635±6,370	76,134±10,826	**77,887±6,123**

7 Conclusion

Achieving beyond-expert performance and improving sample complexity in complicated tasks are two crucial challenges in imitation learning. To address these difficulties, we propose Imitation Learning with Double Exploration (ILDE), which optimizes an uncertainty-regularized discrepancy that combines the distance to the expert policy with cumulative uncertainty during exploration.

Theoretically, we propose ILDE-NPG with a theoretical regret guarantee, a first for imitation learning in MDPs with nonlinear function approximation. Empirically, we introduce a flexible ILDE framework with efficient exploration strategies and demonstrate ILDE's outstanding performance over existing baselines in average return and sample complexity. It is also worth noting that our anaysis cannot be directly applied to the practical version implemented in experiments.

REFERENCES

Alekh Agarwal, Yujia Jin, and Tong Zhang. VO Q L: Towards Optimal Regret in Model-free RL with Nonlinear Function Approximation. In *Annual Conference on Learning Theory (COLT 2023)*, pp. 987–1063, 2023.

Peter Auer, Nicolo Cesa-Bianchi, and Paul Fischer. Finite-time analysis of the multiarmed bandit problem. *Machine learning*, 47:235–256, 2002.

Abdeslam Boularias, Jens Kober, and Jan Peters. Relative entropy inverse reinforcement learning. In *International Conference on Artificial Intelligence and Statistics (AISTATS 2011)*, pp. 182–189, 2011.

Greg Brockman, Vicki Cheung, Ludwig Pettersson, Jonas Schneider, John Schulman, Jie Tang, and Wojciech Zaremba. Openai gym. *arXiv preprint arXiv:1606.01540*, 2016.

Daniel Brown, Wonjoon Goo, Prabhat Nagarajan, and Scott Niekum. Extrapolating beyond suboptimal demonstrations via inverse reinforcement learning from observations. In *International Conference on Machine Learning (ICML 2019)*, pp. 783–792, 2019.

Yuri Burda, Harri Edwards, Deepak Pathak, Amos Storkey, Trevor Darrell, and Alexei A Efros. Large-scale study of curiosity-driven learning. *arXiv preprint arXiv:1808.04355*, 2018.

Qi Cai, Mingyi Hong, Yongxin Chen, and Zhaoran Wang. On the global convergence of imitation learning: A case for linear quadratic regulator. *arXiv preprint arXiv:1901.03674*, 2019.

Jonathan D Chang, Masatoshi Uehara, Dhruv Sreenivas, Rahul Kidambi, and Wen Sun. Mitigating covariate shift in imitation learning via offline data without great coverage. *arXiv preprint arXiv:2106.03207*, 2021.

Minshuo Chen, Yizhou Wang, Tianyi Liu, Zhuoran Yang, Xingguo Li, Zhaoran Wang, and Tuo Zhao. On computation and generalization of generative adversarial imitation learning. In *International Conference on Learning Representations (ICLR 2019)*, 2019.

Paul F Christiano, Jan Leike, Tom Brown, Miljan Martic, Shane Legg, and Dario Amodei. Deep reinforcement learning from human preferences. *Advances in neural information processing systems*, 30, 2017.

Felipe Codevilla, Matthias Müller, Antonio López, Vladlen Koltun, and Alexey Dosovitskiy. End-to-end driving via conditional imitation learning. In *IEEE International Conference on Robotics and Automation (ICRA 2018)*, pp. 4693–4700, 2018.

Chelsea Finn, Sergey Levine, and Pieter Abbeel. Guided cost learning: Deep inverse optimal control via policy optimization. In *International Conference on Machine Learning (ICML 2016)*, pp. 49–58. PMLR, 2016.

Ronan Fruit, Matteo Pirotta, Alessandro Lazaric, and Ronald Ortner. Efficient bias-span-constrained exploration-exploitation in reinforcement learning. In *International Conference on Machine Learning (ICML 2018)*, 2018.

Huiqiao Fu, Kaiqiang Tang, Yuanyang Lu, Yiming Qi, Guizhou Deng, and Chunlin Chen. Ess-InfoGAIL: Semi-supervised Imitation Learning from Imbalanced Demonstrations. 2023.

Ian Goodfellow, Jean Pouget-Abadie, Mehdi Mirza, Bing Xu, David Warde-Farley, Sherjil Ozair, Aaron Courville, and Yoshua Bengio. Generative adversarial networks. *Communications of the ACM*, 63(11):139–144, 2020.

Sijia Gu and Fei Zhu. BAGAIL: Multi-modal imitation learning from imbalanced demonstrations. *Neural Networks*, 174, 2024.

Mikael Henaff, Roberta Raileanu, Minqi Jiang, and Tim Rocktäschel. Exploration via elliptical episodic bonuses. *arXiv preprint arXiv:2210.05805*, 2023.

Todd Hester, Matej Vecerik, Olivier Pietquin, Marc Lanctot, Tom Schaul, Bilal Piot, Dan Horgan, John Quan, Andrew Sendonaris, Ian Osband, et al. Deep q-learning from demonstrations. In *Proceedings of the AAAI conference on artificial intelligence*, volume 32, 2018.

Jonathan Ho and Stefano Ermon. Generative adversarial imitation learning. In *Advances in Neural Information Processing Systems (NeurIPS 2016)*, pp. 4572–4580, 2016.

Thomas Jaksch, Ronald Ortner, and Peter Auer. Near-optimal regret bounds for reinforcement learning. *Journal of Machine Learning Research*, 11:1563–1600, 2010.

Chi Jin, Zhuoran Yang, Zhaoran Wang, and Michael I Jordan. Provably efficient reinforcement learning with linear function approximation. In *Conference on learning theory*, pp. 2137–2143. PMLR, 2020.

Ilya Kostrikov. Pytorch implementations of reinforcement learning algorithms. `https://github.com/ikostrikov/pytorch-a2c-ppo-acktr-gail`, 2018.

Bin Li, Ruofeng Wei, Jiaqi Xu, Bo Lu, Chi Hang Yee, Chi Fai Ng, Pheng Ann Heng, Qi Dou, and Yun Hui Liu. 3D Perception based Imitation Learning under Limited Demonstration for Laparoscope Control in Robotic Surgery. In *IEEE International Conference on Robotics and Automation (ICRA 2022)*, pp. 7664–7670, 2022.

Ziniu Li, Tian Xu, Zeyu Qin, Yang Yu, and Zhi-Quan Luo. Imitation learning from imperfection: Theoretical justifications and algorithms. In *Advances in Neural Information Processing Systems (NeurIPS 2023)*, volume 36, 2024.

Minghuan Liu, Tairan He, Weinan Zhang, Shuicheng Yan, and Zhongwen Xu. Visual imitation learning with patch rewards. In *International Conference on Learning Representations (ICLR 2023)*, 2023.

Qinghua Liu, Gellért Weisz, András György, Chi Jin, and Csaba Szepesvári. Optimistic natural policy gradient: a simple efficient policy optimization framework for online rl. In *Advances in Neural Information Processing Systems (NeurIPS 2023)*, 2024.

Zhihan Liu, Yufeng Zhang, Zuyue Fu, Zhuoran Yang, and Zhaoran Wang. Learning from demonstration: Provably efficient adversarial policy imitation with linear function approximation. In *International Conference on Machine Learning (ICML 2021)*, pp. 14094–14138, 2021.

Francesco Orabona. A modern introduction to online learning. *arXiv preprint arXiv:1912.13213*, 2019.

Takayuki Osa, Naohiko Sugita, and Mamoru Mitsuishi. Online trajectory planning in dynamic environments for surgical task automation. In *Robotics: Science and Systems (RSS 2014)*, pp. 1–9, 2014.

Deepak Pathak, Pulkit Agrawal, Alexei A Efros, and Trevor Darrell. Curiosity-driven exploration by self-supervised prediction. In *International Conference on Machine Learning (ICML 2017)*, pp. 2778–2787, 2017.

Xue Bin Peng, Angjoo Kanazawa, Sam Toyer, Pieter Abbeel, and Sergey Levine. Variational discriminator bottleneck: Improving imitation learning, inverse RL, and GANs by constraining information flow. In *International Conference on Learning Representations (ICLR 2019)*, pp. 1–27, 2019.

Dean A Pomerleau. Alvinn: An autonomous land vehicle in a neural network. In *Advances in Neural Information Processing Systems (NeurIPS 1998)*, 1988.

Daniel Russo and Benjamin Van Roy. Eluder dimension and the sample complexity of optimistic exploration. *Advances in Neural Information Processing Systems*, 26, 2013.

John Schulman, Filip Wolski, Prafulla Dhariwal, Alec Radford, and Oleg Klimov. Proximal policy optimization algorithms. *arXiv preprint arXiv:1707.06347*, 2017.

Younggyo Seo, Lili Chen, Jinwoo Shin, Honglak Lee, Pieter Abbeel, and Kimin Lee. State entropy maximization with random encoders for efficient exploration. In *International Conference on Machine Learning (ICML 2021)*, pp. 9443–9454, 2021.

Lior Shani, Yonathan Efroni, Aviv Rosenberg, and Shie Mannor. Optimistic policy optimization with bandit feedback. In *International Conference on Machine Learning (ICML 2020)*, pp. 8604–8613, 2020.

Lior Shani, Tom Zahavy, and Shie Mannor. Online apprenticeship learning. In *Proceedings of the AAAI Conference on Artificial Intelligence (AAAI 2022)*, pp. 8240–8248, 2022.

Harshinder Singh, Neeraj Misra, Vladimir Hnizdo, Adam Fedorowicz, and Eugene Demchuk. Nearest neighbor estimates of entropy. *American Journal of Mathematical and Management Sciences*, 23 (3-4):301–321, 2003.

Kihyuk Sohn, Honglak Lee, and Xinchen Yan. Learning structured output representation using deep conditional generative models. In *Advances in Neural Information Processing Systems (NeurIPS 2015)*, 2015.

Emanuel Todorov, Tom Erez, and Yuval Tassa. Mujoco: A physics engine for model-based control. In *2012 IEEE/RSJ international conference on intelligent robots and systems*, pp. 5026–5033. IEEE, 2012.

Luca Viano, Angeliki Kamoutsi, Gergely Neu, Igor Krawczuk, and Volkan Cevher. Proximal point imitation learning. In *Advances in Neural Information Processing Systems (NeurIPS 2022)*, pp. 24309–24326, 2022.

Tian Xu, Ziniu Li, and Yang Yu. Error bounds of imitating policies and environments. In *Advances in Neural Information Processing Systems (NeurIPS 2020)*, pp. 15737–15749, 2020.

Zhao-Heng Yin, Weirui Ye, Qifeng Chen, and Yang Gao. Planning for sample efficient imitation learning. In *Advances in Neural Information Processing Systems (NeurIPS 2022)*, volume 35, pp. 2577–2589, 2022.

Xingrui Yu, Yueming Lyu, and Ivor Tsang. Intrinsic reward driven imitation learning via generative model. In *International Conference on Machine Learning (ICML 2020)*, pp. 10925–10935, 2020.

Songyuan Zhang, Zhangjie Cao, Dorsa Sadigh, and Yanan Sui. Confidence-Aware Imitation Learning from Demonstrations with Varying Optimality. In *Advances in Neural Information Processing Systems (NeurIPS 2021)*, pp. 12340–12350, 2021.

Tianhao Zhang, Zoe McCarthy, Owen Jow, Dennis Lee, Xi Chen, Ken Goldberg, and Pieter Abbeel. Deep imitation learning for complex manipulation tasks from virtual reality teleoperation. In *IEEE International Conference on Robotics and Automation (ICRA 2018)*, pp. 5628–5635, 2018.

Yufeng Zhang, Qi Cai, Zhuoran Yang, and Zhaoran Wang. Generative adversarial imitation learning with neural network parameterization: Global optimality and convergence rate. In *International Conference on Machine Learning (ICML 2020)*, pp. 11044–11054, 2020.

Heyang Zhao, Jiafan He, and Quanquan Gu. A nearly optimal and low-switching algorithm for reinforcement learning with general function approximation. *arXiv preprint arXiv:2311.15238*, 2023.

Zhuangdi Zhu, Kaixiang Lin, Bo Dai, and Jiayu Zhou. Self-adaptive imitation learning: Learning tasks with delayed rewards from sub-optimal demonstrations. In *Proceedings of the AAAI conference on artificial intelligence*, volume 36, pp. 9269–9277, 2022.

Brian D Ziebart, Andrew L Maas, J Andrew Bagnell, Anind K Dey, et al. Maximum entropy inverse reinforcement learning. In *AAAI Conference on Artificial Intelligence (AAAI 2008)*, pp. 1433–1438, 2008.

Brian D. Ziebart, J. Andrew Bagnell, and Anind K. Dey. Modeling interaction via the principle of maximum causal entropy. In *International Conference on Machine Learning (ICML 2010)*, pp. 1255–1262, 2010.

A MOTIVATION TABLE

Table 4 illustrates the strengths of each component in ILDE, which helps to explain the motivation of ILDE.

Table 4: Comparison of three reward components with three attributes.

	Stability	Exploration	Imitation
GIRIL reward	++	+	+
Bonus b	+	++	-
VAIL r^k	-	-	++

B AUXILIARY EXPERIMENTAL DETAILS

B.1 DEMONSTRATION LENGTHS IN THE ATARI ENVIRONMENT

Table 5 compares the lengths of one-life demonstrations and full-episode demonstrations in Atari games. In the experiments, we only use 10% of the one-life demonstrations for imitation learning, which is more challenging than previous work in learning with limited demonstrations (Yu et al., 2020).

Table 5: Demonstration lengths in the Atari environment.

Atari Games	One-life Demo.		Full-episode Demo.	
	Length	# Life	Length	# Life
Beam Rider	702	1	1,412	3
Demon Attack	2,004	1	11,335	4
Battle Zone	260	1	1,738	5
Q*bert	787	1	1,881	4
Krull	662	1	1,105	3
Star Gunner	118	1	2,117	5

B.2 EXPERIMENTAL SETUP AND ADDITIONAL RESULTS

This subsection presents details of VAIL, GIRIL, state entropy bonus, experimental setup, and additional results.

B.2.1 DETAILS OF THE VARIATIONAL ADVERSARIAL IMITATION LEARNING (VAIL)

Generative adversarial imitation learning (GAIL) (Ho & Ermon, 2016) regards imitation learning as a distribution matching problem, and updates policy using adversarial learning (Goodfellow et al., 2020). Previous work has demonstrated that GAIL does not work well in high-dimensional environments like Atari games (Brown et al., 2019). Variational adversarial imitation learning (VAIL) (Peng et al., 2019) improves GAIL by compressing the information via a variational information bottleneck (VDB). VDB constrains information flow in the discriminator by means of an information bottleneck. By enforcing a constraint on the mutual information between the observations and the discriminator's internal representation, VAIL significantly outperforms GAIL by optimizing the following objective:

$$\min_{D_\theta, E'} \max_{\beta \geq 0} \mathbb{E}_{(s,a)\sim\tau^E}\Big[\mathbb{E}_{z\sim E'(z|s)}\big[\log(-D_\theta(z))\big]\Big] + \mathbb{E}_{(s,a)\sim\pi^k}\Big[\mathbb{E}_{z\sim E'(z|s)}\big[-\log(1-D_\theta(z))\big]\Big] + \beta\mathbb{E}_{s\sim\tilde{\pi}}\big[d_{KL}(E'(z|s)|r^k) - I_c\big], \tag{B.1}$$

where $\widetilde{\pi} = \frac{1}{2}\pi^E + \frac{1}{2}\pi^k$ represents a mixture of the expert policy and the agent's policy, E' is the encoder for VDB, β is the scaling weight, and I_c is the information constraint. The reward for π is then specified by the discriminator $r_t = -\log\big(1 - D_\theta(\boldsymbol{\mu}_{E'}(s))\big)$.

B.2.2 Details of the generative intrinsic reward driven imitation learning (GIRIL)

Previous inverse reinforcement learning (IRL) methods usually fail to achieve expert-level performance when learning with limited demonstrations in high-dimensional environments. To address this challenge, Yu et al. (2020) proposed generative intrinsic reward-driven imitation learning (GIRIL) to empower the agent with the demonstrator's intrinsic intention and better exploration ability. This was achieved by training a novel reward model to generate intrinsic reward signals via a generative model. Specifically, GIRIL leverages a conditional VAE (Sohn et al., 2015) to combine a backward action encoding model and a forward dynamics model into a single generative model. The module is composed of several neural networks, including recognition network $q_\phi(z|s_t, s_{t+1})$, a generative network $p_\theta(s_{t+1}|z, s_t)$, and prior network $p_\theta(z|s_t)$. GIRIL refers to the recognition network (i.e. the probabilistic *encoder*) as a backward action encoding model, and the generative network (i.e. the probabilistic *decoder*) as a forward dynamics model. Maximizing the following objective to optimize the module:

$$\begin{aligned} J(p_\theta, q_\phi) = \mathbb{E}_{q_\phi(z|s_t,s_{t+1})}[\log p_\theta(s_{t+1}|z, s_t)] - \mathrm{KL}(q_\phi(z|s_t, s_{t+1})\|p_\theta(z|s_t)) \\ - \alpha d_{KL}(q_\phi(\widehat{a}_t|s_t, s_{t+1})|\pi_E(a_t|s_t)] \end{aligned} \tag{B.2}$$

where z is the latent variable, $\pi_E(a_t|s_t)$ is the expert policy distribution, $\widehat{a}_t = \mathrm{Softmax}(z)$ is the transformed latent variable, α is a positive scaling weight. The reward model will be pre-trained on the demonstration data and used for inferring intrinsic rewards for the policy data. The intrinsic reward is calculated as the reconstruction error between $\widehat{s}_{t+1}$ and s_{t+1}:

$$r_t = \|\widehat{s}_{t+1} - s_{t+1}\|_2^2 \tag{B.3}$$

where $\|\cdot\|_2$ denotes the L2 norm, $\widehat{s}_{t+1} = decoder(a_t, s_t)$.

B.2.3 Details of state entropy bonus

State entropy maximization has been demonstrated to be a simple and compute-efficient method for exploration (Seo et al., 2021). The key idea for this method to work in a high-dimensional environment is to utilize a k-nearest neighbor state entropy estimator in the state representation space.

k-nearest neighbor entropy estimator. Let X be a random variable with a probability density function p whose support is a set $\mathcal{X} \subset \mathbb{R}^d$. Then its differential entropy is given by

$$\mathcal{H}(X) = -\int_{\mathcal{X}} p(x) \log p(x) dx.$$

Since estimating p is not tractable for high-dimensional data, a particle-based k-nearest neighbors (k-NN) entropy estimator (Singh et al., 2003) can be used:

$$\begin{aligned} \mathcal{H}(X) &\approx \frac{1}{N}\sum_{i=1}^{N} \log \frac{N \cdot \|x_i - x_i^{k-\mathrm{NN}}\|_2^d \cdot \widehat{\pi}^{\frac{d}{2}}}{k \cdot \Gamma(\frac{d}{2}+1)} + C_k \\ &\propto \frac{1}{N}\sum_{i=1}^{N} \log \|x_i - x_i^{k-\mathrm{NN}}\|_2, \end{aligned} \tag{B.4}$$

where $x_i^{k-\mathrm{NN}}$ is the k-nearest neighbor of x_i within a set of N representations $\{x_1, x_2, \cdots, x_N\}$, Γ is the gamma function, $\widehat{\pi}$ refers to an estimate of the number π (as opposed to the policy), and $\log(k - \psi)$ where ψ is the digamma function. **State entropy estimate as bonus.** Following Seo et al. (2021), we define the bonus to be proportional to the state entropy estimate in (B.4),

$$b(s_i) := \log(\|y_i - y_i^{k-\mathrm{NN}}\|_2 + 1), \tag{B.5}$$

where $y_i = f(s_i)$ is a fixed representation from a state feature extractor f and $y_i^{k-\mathrm{NN}}$ is the k-nearest neighbor of y_i within a set of N representations $\{y_1, y_2, \cdots, y_N\}$. The use of a fixed representation

space produces a more stable intrinsic reward since the distance between a given pair of states does not change during training (Seo et al., 2021). In our implementation, we use the identity function as the feature extractor f.

B.2.4 EXPERIMENTAL SETUP

For the GIRIL and ILDEs, our first step was to train a reward model for each game using the 10% of a one-life demonstration. The training was conducted with the Adam optimizer at a learning rate of 3e-4 and a mini-batch size of 32 for 1,000 epochs. In each training epoch, we sampled a mini-batch of data every four states. To evaluate the quality of our learned reward, we used the trained reward learning module to produce intrinsic rewards for policy data and trained a policy to maximize the inferred intrinsic rewards via PPO. For VAIL, we trained the discriminator using the Adam optimizer with a learning rate of 3e-4. The discriminator was updated at every policy step. We trained the PPO policy for all imitation learning methods for 50 million steps. We compare ILDE with baselines in the measurement of average return and sample efficiency. The average return was measured using the true rewards in the environment. We measured the sample efficiency based on the step after which an imitation learning method can continuously outperform the expert until the training ends. All the experiments are executed in an NVIDIA A100 GPU with 40 GB memory.

Network architectures. We implement our ILDE and all the baselines in the feature space of a state feature extractor f with 3 convolutional layers. The dimension of the state feature is 5184. In the state feature space, we use 3-layer MLPs to implement the discriminator for VAIL and the encoder and decoder for GIRIL. For a fair comparison, we used an identical policy network for all methods. We used the actor-critic approach for training PPO policy for all the imitation learning methods. Table 6 shows the architecture details of the state feature extractor and actor-critic network. Table 7 shows the MLP architectures, i.e., GIRIL's *encoder* and *decoder* and VAIL's discriminator.

Table 6: Architectures of state feature extractor and actor-critic network for Atari games.

State feature extractor	Actor-Critic network	
$4 \times 84 \times 84$ States	$4 \times 84 \times 84$ States	
3×3 conv, 32 LeakyReLU 3×3 conv, 32 LeakyReLU 3×3 conv, 64 LeakyReLU	8×8 conv, 32, stride 4, ReLU 4×4 conv, 64, stride 2, ReLU 3×3 conv, 32, stride 1, ReLU	
flatten $64 \times 9 \times 9 \rightarrow 5184$	dense $32 \times 7 \times 7 \rightarrow 512$ Categorical Distribution	dense $32 \times 7 \times 7 \rightarrow 1$
State features	Actions	Values

Table 7: Architectures of MLP-based GIRIL's *encoder* and *decoder*, and VAIL's discriminator.

GIRIL		VAIL
encoder	*decoder*	discriminator
5184 State features and next-state features	Actions and 5184 State features	Actions and 5184 State features
dense 5184×2 $\rightarrow$ 1024, LeakyReLU dense 1024 $\rightarrow$ 1024, LeakyReLU dense 1024 $\rightarrow \boldsymbol{\mu}$, dense 1024 $\rightarrow \boldsymbol{\sigma}$ reparameterization $\rightarrow$ #Actions	dense 5182+#Actions $\rightarrow$ 1024, LeakyReLU dense 1024 $\rightarrow$ 1024, LeakyReLU dense 1024 $\rightarrow$ 5184	dense 5182 $\rightarrow$ 1024, LeakyReLU dense 1024 $\rightarrow$ 1024, LeakyReLU split 1024 into 512, 512 dense 512 $\rightarrow \boldsymbol{\mu}_{E'}$, dense 512 $\rightarrow \boldsymbol{\sigma}_{E'}$ reparameterization $\rightarrow$ 1
Latent variables	5184 Predicted next state features	$\boldsymbol{\mu}_{E'}$, $\boldsymbol{\sigma}_{E'}$, discrimination

Hyperparameter settings. We implemented all the imitation learning methods and conducted experiments based on the GitHub repository by Kostrikov (2018). Additional parameter settings are explained in Table 8.

B.2.5 ADDITIONAL RESULTS

To better illustrate the significance of the improvement of ILDE against the expert demonstrator, we normalized the results by stating that the expert was 1.0. The normalized results are summarized in Table 9. On average, VAIL is worse than the expert, only outperforming the expert in Krull. GIRIL

Table 8: Hyperparameter settings for Atari games.

Parameter	Setting
Actor-critic learning rate	2.5e-4, linear decay
PPO clipping	0.1
Reward model learning rate	3e-4
Discount factor	0.99
GAE Lambda	0.95
Critic loss coefficient	0.5
Entropy regularisation	0.01
Epochs per batch	4
Batch size	32×128 (parallel workers $\times$ time steps)
Mini batch size	32
Evaluation frequency	every 200 policy updates
GIRIL objective α	100.0
Mini batch size for training the reward model	32
Total training epoch of reward model	$1,000$
VAIL's bottleneck loss weight β	1.0
Information constraint I_c	0.2
λ in Algorithm 3	10.0

archives a performance that is 4.87 times the expert, performing the best in Q*bert. ILDE is the best, achieving a performance that is 5.33 times of the expert. Figure 1 illustrates the learning curves of imitation learning methods in the 6 Atari games over 10 random seeds.

Table 9: Average performance improvements of imitation learning methods versus the expert demonstrator. The expert performance is regarded as 1.0. "Improve vs Expert" denotes the average improvements of IL methods versus the expert across 6 Atari games.

Atari Games	Expert	VAIL (r^k)	GIRIL	ILDE w/o b	ILDE w/o r^k	ILDE
BeamRider	1.0	0.05	4.44	4.44	5.97	5.97
DemonAttack	1.0	0.11	8.21	8.90	6.91	7.31
BattleZone	1.0	0.23	1.12	0.81	1.95	2.64
Q*bert	1.0	0.60	12.25	4.31	8.67	11.30
Krull	1.0	1.22	3.21	2.56	4.22	3.64
StarGunner	1.0	0.01	0.02	0.02	0.73	1.13
Improve vs Expert	1.0	0.37	4.87	3.50	4.71	**5.33**

Additionally, we summarize the sample efficiency improvements of VAIL and ILDE methods versus GIRIL in Table 11. We calculate the improvement ratio of sample efficiency based on the results in Table 10 in Section 6. Recall that Table 10 compares the sample efficiency of ILDE and other baselines. The results are the minimal steps after which imitation learning methods continuously outperform the experts until the end. For better illustration, we present the ratio of these steps over 50 million steps. The lower the ratio, the better the sample efficiency. '-' indicates the method failed to outperform GIRIL in 50 million steps. To quantitatively compare the sample efficiency improvements of ILDEs versus GIRIL, we regard the results indicated by '-' as 100% of the total time steps (50 million), and calculate the improvement ratios on sample efficiency. "Improve vs GIRIL" presents the average sample efficiency improvements over 6 Atari games. ILDE archives the highest sample efficiency improvements of 26.83% compared with GIRIL. The improvement ratio of sample efficiency for each imitation learning method compared with GIRIL is summarized in Table 11. The sample efficiency of VAIL in outperforming experts is much worse than GIRIL and ILDE variants. ILDE shows impressive sample efficiency improvement in BattleZone, outperforming GIRIL by 90.06%.

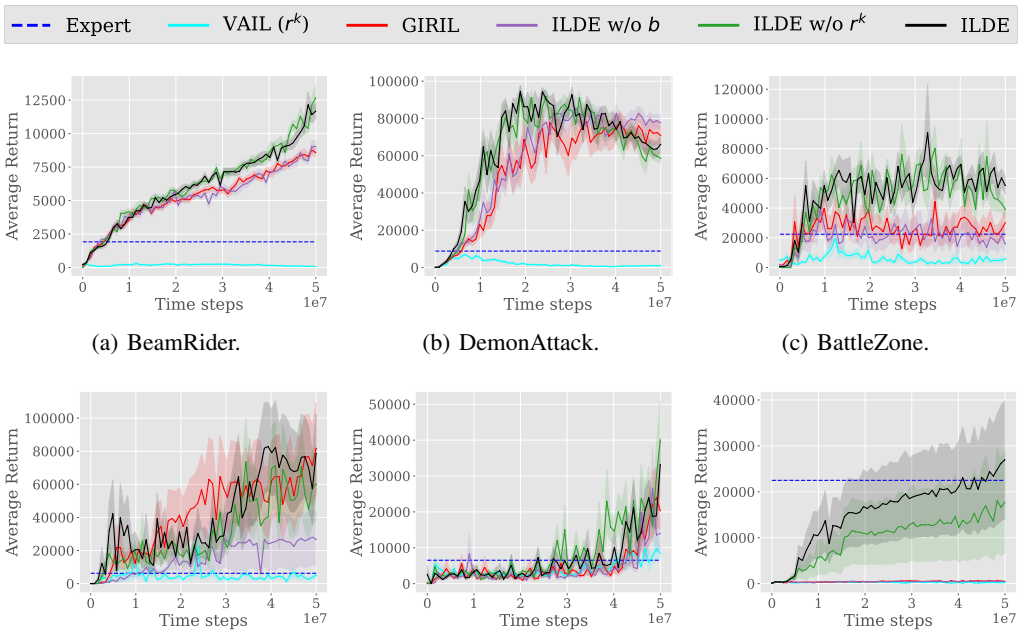

(a) BeamRider. (b) DemonAttack. (c) BattleZone.

(d) Q*bert. (e) Krull. (f) StarGunner.

Figure 1: Average return vs. number of simulation steps on Atari games. The solid lines show the mean performance over 10 random seeds. The shaded area represents the standard deviation from the mean. The blue dotted line denotes the average return of the expert demonstrator. The area above the blue dotted line means performance beyond the expert.

Table 10: The ratio of steps indicating the sample efficiency of imitation learning methods. The ratio is calculated on the minimal step, after which an imitation learning method can continuously outperform the experts until the end. A smaller step ratio means better sample efficiency. "Games>GIRIL" denotes the number and ratio of games that an imitation learning method has better sample efficiency than GIRIL. The better-than-GIRIL results in terms of sample efficiency are in bold. "Improve vs Expert" denotes the average ratio of sample efficiency improvements of IL methods versus GIRIL in outperforming the expert across the 6 Atari games. '-' indicates the method failed to outperform GIRIL in 50 million steps.

Atari Games	VAIL (r^k)	GIRIL	ILDE w/o b	ILDE w/o r^k	ILDE
BeamRider	-	9.84%	**8.20%**	9.84%	11.48%
DemonAttack	-	13.12%	**9.84%**	**11.48%**	**8.20%**
BattleZone	-	98.31%	-	**11.48%**	**9.84%**
Qbert	-	9.84%	21.31%	**6.56%**	**8.20%**
Krull	96.67%	85.20%	91.76%	**72.10%**	**83.57%**
StarGunner	-	-	-	-	**93.40%**
Games>GIRIL	0 / 0%	0 / 0%	2 / 33.3%	4 / 66.7%	**5 / 83.3%**
Improve vs GIRIL	-418.32%	0%	-14.05%	24.92%	22.68%

B.2.6 Continuous control tasks

Except for the above evaluation on the Atari games with high-dimensional state space and discrete action space, we also evaluated our method on continuous control tasks where the state space is low-dimensional and the action space is continuous. The continuous control tasks were from MuJoCo (Todorov et al., 2012).

Demonstrations. We used the demonstrations from the open-source repository "pytorch-a2c-ppo-acktr-gail" (Kostrikov, 2018). We compare ILDE with VAIL and GIRIL on the continuous control

Table 11: Sample efficiency improvements of VAIL and ILDE methods versus the GIRIL. "Improve vs GIRIL" denotes the average improvements of IL methods versus the GIRIL across 6 Atari games.

Atari Games	VAIL (r^k)	GIRIL	ILDE w/o b	ILDE w/o r^k	ILDE
BeamRider	-916.26%	0%	16.67%	0%	-16.67%
DemonAttack	-662.21%	0%	25%	12.5%	37.5%
BattleZone	-1.71%	0%	-1.72%	88.32%	90.06%
Q*bert	-916.26%	0%	-116.57%	33.33%	16.67%
Krull	-13.46%	0%	-7.69%	15.37%	1.91%
StarGunner	0%	0%	0%	0%	6.6%
Improve vs GIRIL	-418.32%	0%	-14.05%	24.92%	**26.83%**

tasks (i.e., Reacher, Hopper, Walker2d, and HumanoidStandup) with 4 trajectories in the demonstration for each task.

Experimental setups. Similar to the setups in Atari games, we need to pretrain a reward model for GIRIL and ILDE using the demonstrations. The training was conducted with the Adam optimizer at a learning rate of 3e-4 and a mini-batch size of 32 for 10,000 epochs. In each training epoch, we sampled a mini-batch of data every 20 states. To evaluate the quality of our learned reward, we used the trained reward learning module to produce intrinsic rewards for policy data and trained a policy to maximize the inferred intrinsic rewards via PPO. For VAIL, we trained the discriminator using the Adam optimizer with a learning rate of 3e-4. The discriminator was updated at every policy step. We trained the PPO policy for all imitation learning methods for 10 million steps. We compare ILDE with baselines in the measurement of average return. The average return was measured using the true rewards in the environment. All the experiments are executed in an NVIDIA A100 GPU with 40 GB memory.

Network architectures. We use 3-layer MLPs to implement the discriminator for VAI, and the encoder and the decoder for GIRIL and ILDE. For a fair comparison, we used an identical policy network for all methods. We used the actor-critic approach for training PPO policy for all the imitation learning methods. The number of hidden layers in each MLP is 100. Table 12 shows the architecture details of the actor-critic network for MuJoCo tasks. Table 13 shows the MLP architectures, i.e., GIRIL's *encoder* and *decoder* and VAIL's discriminator.

Table 12: Architectures of the actor-critic network for MuJoCo tasks. $\dim(\mathcal{S})$ and $\dim(\mathcal{A})$ represent the state dimension and action dimension, respectively.

Actor-Critic network	
$1 \times \dim(\mathcal{S})$ States	
dense $\dim(\mathcal{S}) \rightarrow 100$, Tanh dense $100 \rightarrow 100$, Tanh	
dense $100 \rightarrow \dim(\mathcal{A})$ Gaussian Distribution	dense $100 \rightarrow 1$
Actions	Values

Table 13: Architectures of MLP-based GIRIL's *encoder* and *decoder*, and VAIL's discriminator.

GIRIL		VAIL
encoder	*decoder*	discriminator
$1 \times \dim(\mathcal{S})$ States and Next State	$1 \times \dim(\mathcal{A})$ Actions and $1 \times \dim(\mathcal{S})$ States	$1 \times \dim(\mathcal{A})$ Actions and $1 \times \dim(\mathcal{S})$ States
dense $\dim(\mathcal{S}) \times 2 \rightarrow 100$, Tanh dense $100 \rightarrow 100$, Tanh dense $100 \rightarrow \boldsymbol{\mu}$, dense $100 \rightarrow \boldsymbol{\sigma}$ reparameterization $\rightarrow \dim(\mathcal{A})$	dense $\dim(\mathcal{S})$+$\dim(\mathcal{A}) \rightarrow 100$, Tanh dense $100 \rightarrow 100$, Tanh dense $100 \rightarrow \dim(\mathcal{S})$	dense $\dim(\mathcal{S}) \rightarrow 100$, Tanh dense $100 \rightarrow 100$, Tanh split 100 into 50, 50 dense $50 \rightarrow \boldsymbol{\mu}_{E'}$, dense $50 \rightarrow \boldsymbol{\sigma}_{E'}$ reparameterization $\rightarrow 1$
Latent variables	$\dim(\mathcal{S})$ Predicted next states	$\boldsymbol{\mu}_{E'}$, $\boldsymbol{\sigma}_{E'}$, discrimination

Hyperparameter settings. Table 14 summarized the parameter settings for MuJoCo tasks.

Table 14: Hyperparameter settings for MuJoCo tasks.

Parameter	Setting
Actor-critic learning rate	3e-4, linear decay
PPO clipping	0.1
Reward model learning rate	3e-4
Discount factor	0.99
GAE Lambda	0.95
Critic loss coefficient	0.5
Entropy regularisation	0.0
Epochs per batch	10
Batch size	32×2048 (parallel workers $\times$ time steps)
Mini batch size	32
Evaluation frequency	every 6 policy updates
GIRIL objective α	0.01
Mini batch size for training the reward model	32
Total training epoch of reward model	$10,000$
VAIL's bottleneck loss weight β	1.0
Information constraint I_c	0.2
λ in Algorithm 3	10.0

Results. Figure 2 illustrates the curves of VAIL, GIRIL, and ILDE in the four continuous control tasks. The ablations results on MuJoCo are illustrated in Figure 3.

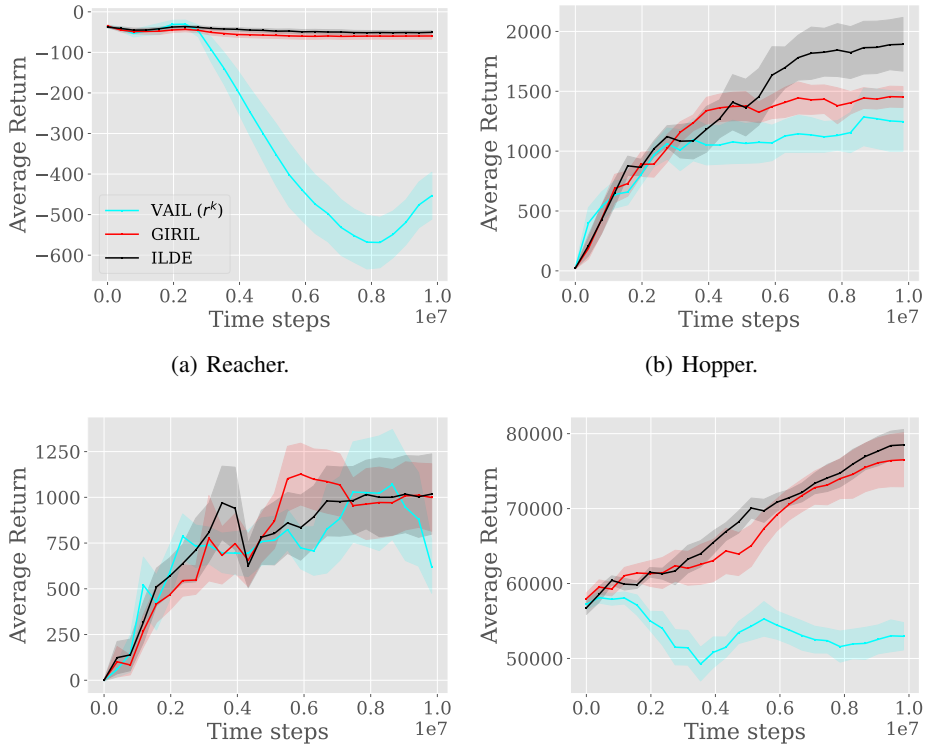

(a) Reacher. (b) Hopper.

(c) Walker2d. (d) HumanoidStandup.

Figure 2: Average return vs. the number of simulation steps on MuJoCo tasks. The solid lines show the mean performance over 10 random seeds. The shaded area represents the standard deviation from the mean.

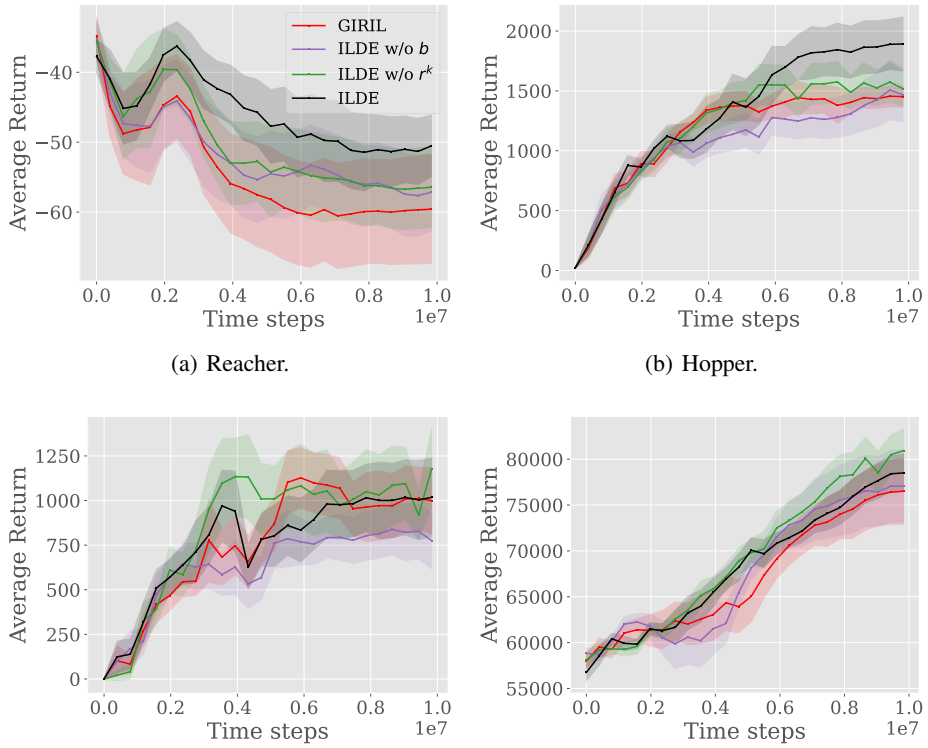

(a) Reacher. (b) Hopper.

(c) Walker2d. (d) HumanoidStandup.

Figure 3: Ablations on MuJoCo tasks. Average return vs. the number of simulation steps on MuJoCo tasks. The solid lines show the mean performance over 10 random seeds. The shaded area represents the standard deviation from the mean.

C Proof of Theorem 4.7

Our proof structure for Theorem 4.7 largely adapts from the proofs in Liu et al. (2024). However, our analysis different from theirs in three aspects: (1) we consider imitation learning, where the reward is time-varying, (2) we consider MDPs with generalized Eluder dimension, which is slightly more general than Eluder dimension (Russo & Van Roy, 2013) as shown in Zhao et al. (2023), and (3) the analysis leads to a sublinear batch-regret, which is stronger than a sample complexity bound.

First, we have the following extended value difference lemma.

Lemma C.1 (Value difference lemma)**.** For any policy π, the value functions $\{V_h^k\}_{h=1}^H$ and $\{Q_h^k\}_{h=1}^H$ returned by OPE$(\pi, \mathcal{D}, \widetilde{r})$ satisfy the following equation,

$$V_{1,\pi}^{\widetilde{r}}(s_1) - V_1^k(s_1) = \sum_{h=1}^H \mathbb{E}_{s_h\sim\pi}\left[\langle Q_h^k(s_h,\cdot), \pi_h(\cdot|s_h) - \pi_h^k(\cdot|s_h)\rangle\right] - \sum_{h=1}^H \mathbb{E}_{(s_h,a_h)\sim\pi}\left[Q_h^k(s_h,a_h) - \widetilde{r}(s_h,a_h) - \mathbb{P}_h V_{h+1}^k(s_h,a_h)\right].$$

Proof. For any $h \in [H]$, $s \in \mathcal{S}$, we have

$$\begin{aligned} V_{h,\pi}^{\widetilde{r}}(s) - V_h^k(s) &= \langle Q_{h,\pi}^{\widetilde{r}}(s,\cdot), \pi_h(\cdot|s)\rangle - \langle Q_h^k(s,\cdot), \pi_h^k(\cdot|s)\rangle \\ &= \langle Q_{h,\pi}^{\widetilde{r}}(s,\cdot) - Q_h^k(s,\cdot), \pi_h(\cdot|s)\rangle - \langle Q_h^k(s,\cdot), \pi_h^k(\cdot|s) - \pi_h(\cdot|s)\rangle \\ &= \langle \mathbb{P}_h V_{h+1,\pi}^{\widetilde{r}}(s,\cdot) - \mathbb{P}_h V_{h+1}^k(s,\cdot), \pi_h(\cdot|s)\rangle - \langle Q_h^k(s,\cdot), \pi_h^k(\cdot|s) - \pi_h(\cdot|s)\rangle \\ &\quad - \langle Q_h^k(s,\cdot) - \widetilde{r}(s,\cdot) - \mathbb{P}_h V_{h+1}^k(s,\cdot), \pi_h(\cdot|s)\rangle, \end{aligned} \tag{C.1}$$

where the first equality follows from the definition of the value functions V_h^k and Q_h^k, the last equality follows from the Bellman equation for the state-action value function $Q_{h,\pi}$ in (3.2). From (C.1) we further obtain that for any $h \in [H]$, policy π,

$$\mathbb{E}_{s_h\sim\pi}\big[V_{h,\pi}^{\widetilde{r}}(s_h) - V_h^k(s_h)\big] - \mathbb{E}_{s_h\sim\pi}\big[V_{h+1,\pi}^{\widetilde{r}}(s_{h+1}) - V_{h+1}^k(s_{h+1})\big]$$
$$= \mathbb{E}_{s_h\sim\pi}\big[\langle Q_h^k(s_h,\cdot), \pi_h(\cdot|s_h) - \pi_h^k(\cdot|s_h)\rangle\big] - \mathbb{E}_{s_h\sim\pi}\big[\langle Q_h^k(s_h,\cdot) - \widetilde{r}(s_h,\cdot) - \mathbb{P}_h V_{h+1}^k(s_h,\cdot), \pi_h(\cdot|s_h)\rangle\big].$$

Taking the sum over $h \in [H]$ yields the following result,

$$\begin{aligned}
&V_{1,\pi}^{\widetilde{r}}(s_1) - V_1^k(s_1)\\
&= \sum_{h=1}^H \mathbb{E}_{s_h\sim\pi}\big[\langle Q_h^k(s_h,\cdot), \pi_h(\cdot|s_h) - \pi_h^k(\cdot|s_h)\rangle\big]\\
&\quad - \sum_{h=1}^H \mathbb{E}_{s_h\sim\pi}\big[\langle Q_h^k(s_h,\cdot) - \widetilde{r}(s_h,\cdot) - \mathbb{P}_h V_{h+1}^k(s_h,\cdot), \pi_h(\cdot|s_h)\rangle\big]\\
&= \sum_{h=1}^H \mathbb{E}_{s_h\sim\pi}\big[\langle Q_h^k(s_h,\cdot), \pi_h(\cdot|s_h) - \pi_h^k(\cdot|s_h)\rangle\big] - \sum_{h=1}^H \mathbb{E}_{(s_h,a_h)\sim\pi}\big[Q_h^k(s_h,a_h) - \widetilde{r}(s_h,a_h) - \mathbb{P}_h V_{h+1}^k(s_h,a_h)\big].
\end{aligned}$$

□

Lemma C.2 (Lemma 17, Shani et al. 2020)**.** For any policy π, $s \in \mathcal{S}$, $h \in [H]$, we have

$$\sum_{k=1}^K \big[\langle Q_h^k(s,\cdot), \pi_h(\cdot|s) - \pi_h^k(\cdot|s)\rangle\big] \le \log|\mathcal{A}|/\eta + \eta H^2 K/2.$$

Lemma C.3. Suppose Assumption 4.5 holds. Then with probability at least $1-\delta$, for all $h \in [H]$, $s \in \mathcal{S}$, $a \in \mathcal{A}$, we have

$$\big|\widehat{f}_{k,h}(s,a) - \mathbb{P}_h V_{k,h+1}(s,a)\big| \le \sqrt{8H^2\log(H\cdot\mathcal{N}_{\mathcal{F}}(\epsilon_{\mathcal{F}})/\delta) + 4\epsilon_{\mathcal{F}}N + \gamma}\cdot D_{\mathcal{F}_h}((s,a);\mathcal{D}_h).$$

Proof. We have

$$\begin{aligned}
&\sum_{(s_h,a_h)\in\mathcal{D}_h^k} \big(\widehat{f}_{k,h}(s_h,a_h) - \mathbb{P}_h V_{k,h+1}(s_h,a_h)\big)^2\\
&\quad + 2\sum_{(s_h,a_h)\in\mathcal{D}_h^k} \big(\widehat{f}_{k,h}(s_h,a_h) - \mathbb{P}_h V_{k,h+1}(s_h,a_h)\big)\cdot\big(V_{k,h+1}(s_{h+1}) - \mathbb{P}_h V_{k,h+1}(s_h,a_h)\big)\\
&= \sum_{(s_h,a_h)\in\mathcal{D}_h^k} \big(\widehat{f}_{k,h}(s_h,a_h) - V_{k,h+1}(s_{h+1})\big)^2 - \sum_{(s_h,a_h)\in\mathcal{D}_h^k} \big(V_{k,h+1}(s_{h+1}) - \mathbb{P}_h V_{k,h+1}(s_h,a_h)\big)^2 \le 0,
\end{aligned}$$

where the last inequality follows from the definition of $\widehat{f}_{k,h}$ in Algorithm 2.

Then it follows that for all $h \in [H]$,

$$\begin{aligned}
&\sum_{(s_h,a_h)\in\mathcal{D}_h^k} \big(\widehat{f}_{k,h}(s_h,a_h) - \mathbb{P}_h V_{k,h+1}(s_h,a_h)\big)^2\\
&\quad \le 2\sum_{(s_h,a_h)\in\mathcal{D}_h^k} \big(\widehat{f}_{k,h}(s_h,a_h) - \mathbb{P}_h V_{k,h+1}(s_h,a_h)\big)\cdot\big(\mathbb{P}_h V_{k,h+1}(s_h,a_h) - V_{k,h+1}(s_{h+1})\big).
\end{aligned} \tag{C.2}$$

Note that $V_{k,h+1}$ is a function only depends on data in $\mathcal{D}_{h+1}, \mathcal{D}_{h+2}, \cdots, \mathcal{D}_H$. Hence the right-hand side of the above inequality is a martingale difference sequence.

Consider a function $f \in \mathcal{C}(\mathcal{F}_h, \epsilon_{\mathcal{F}}) \subseteq \mathcal{F}_h$. By Lemma D.2, we have with probability at least $1 - \delta/(H\cdot\mathcal{N}_{\mathcal{F}}(\epsilon_{\mathcal{F}}))$,

$$\begin{aligned}
&\sum_{(s_h,a_h)\in\mathcal{D}_h^k} \big(f(s_h,a_h) - \mathbb{P}_h V_{k,h+1}(s_h,a_h)\big)\cdot\big(\mathbb{P}_h V_{k,h+1}(s_h,a_h) - V_{k,h+1}(s_{h+1})\big)\\
&\quad \le \frac{1}{4}\sum_{(s_h,a_h)\in\mathcal{D}_h^k} \big(f(s_h,a_h) - \mathbb{P}_h V_{k,h+1}(s_h,a_h)\big)^2 + 2H^2\log(H\cdot\mathcal{N}_{\mathcal{F}}(\epsilon_{\mathcal{F}})/\delta).
\end{aligned} \tag{C.3}$$

Combining (C.2) and (C.3) and from the definition of $\epsilon_{\mathcal{F}}$-net $\mathcal{C}(\mathcal{F}_h, \epsilon_{\mathcal{F}})$, we have with probability at least $1-\delta/H$,

$$\sum_{(s_h,a_h)\in\mathcal{D}_h^k} \left(\widehat{f}_{k,h}(s_h,a_h) - \mathbb{P}_h V_{k,h+1}(s_h,a_h)\right)^2 \leq 8H^2 \log(H\cdot\mathcal{N}_{\mathcal{F}}(\epsilon_{\mathcal{F}})/\delta) + 4\epsilon_{\mathcal{F}} H\cdot N/H.$$

By the definition of $D^2_{\mathcal{F}_h}$, we have with probability at least $1-\delta/H$,

$$\left|\widehat{f}_{k,h}(s,a) - \mathbb{P}_h V_{k,h+1}(s,a)\right| \leq \sqrt{8H^2\log(H\cdot\mathcal{N}_{\mathcal{F}}(\epsilon_{\mathcal{F}})/\delta) + 4\epsilon_{\mathcal{F}} N + \gamma}\cdot D_{\mathcal{F}_h}((s,a);\mathcal{D}_h),$$

from which we can complete the proof by applying the union bound over $h\in[H]$. □

Lemma C.4. For any policy π, suppose we sample N trajectories $\mathcal{D} = \{s_h^{(i)}, a_h^{(i)}\}_{h\in[H],i\in[N]}$. Then, with probability at least $1-\delta$, we have

$$\mathbb{E}_{z_h\sim\pi}\left[D_{\mathcal{F}_h}(z_h;\mathcal{D})\right] = O\left(\sqrt{\frac{1}{N}\cdot\frac{H^2+\gamma}{\gamma}\dim_N(\mathcal{F}_h)\log(1/\delta)}\right).$$

Proof. It follows from the definition of $\dim_N(\mathcal{F}_h)$ that

$$\dim_N(\mathcal{F}_h) \geq \sum_{i=1}^N \min\left(1, D^2_{\mathcal{F}_h}(z_h^{(i)}; z_h^{[i-1]})\right). \tag{C.4}$$

From Definition 4.3, we further have the following upper bound for cumulative uncertainty,

$$\begin{aligned}\sum_{i=1}^N D^2_{\mathcal{F}_h}(z_h^{(i)}; z_h^{[i-1]}) &\leq \frac{H^2}{\gamma}\sum_{i=1}^N \mathbb{1}\left(D^2_{\mathcal{F}_h}(z_h^{(i)}; z_h^{[i-1]}) > 1\right) + \sum_{i=1}^N \min\left(1, D^2_{\mathcal{F}_h}(z_h^{(i)}; z_h^{[i-1]})\right)\\ &\leq \left(\frac{H^2}{\gamma}+1\right)\cdot\dim_N(\mathcal{F}_h).\end{aligned} \tag{C.5}$$

Thus,

$$\sum_{i=1}^N D_{\mathcal{F}_h}(z_h^{(i)}; z_h^{[i-1]}) \leq \sqrt{N\cdot\left(\frac{H^2}{\gamma}+1\right)\cdot\dim_N(\mathcal{F}_h)} \tag{C.6}$$

by AM-GM inequality.

On the other hand, from Azuma-Hoeffding inequality (Lemma D.1), we have with probability at least $1-\delta$,

$$\begin{aligned}\sum_{i=1}^N D_{\mathcal{F}_h}(z_h^{(i)}; z_h^{[i-1]}) &\geq \sum_{i=1}^N \mathbb{E}_{z_h\sim\pi}\left[D_{\mathcal{F}_h}(z_h; z_h^{[i-1]})\right] - O\left(\frac{H}{\sqrt{\gamma}}\sqrt{N\log(1/\delta)}\right)\\ &\geq N\cdot\mathbb{E}_{z_h\sim\pi}\left[D_{\mathcal{F}_h}(z_h;\mathcal{D})\right] - O\left(\frac{H}{\sqrt{\gamma}}\sqrt{N\log(1/\delta)}\right)\end{aligned} \tag{C.7}$$

Substituting (C.6) into (C.7) yields:

$$\mathbb{E}_{z_h\sim\pi}\left[D_{\mathcal{F}_h}(z_h;\mathcal{D})\right] = O\left(\sqrt{\frac{1}{N}\cdot\frac{H^2+\gamma}{\gamma}\dim_N(\mathcal{F}_h)\log(1/\delta)}\right). \tag{C.8}$$

□

Lemma C.5 (Lemma 3, Liu et al. 2024)**.** Let t_k be the index of the last policy which is used to collect fresh data at iteration k. Suppose we choose η and m such that $\eta m \leq 1/H^2$, then for any $k\in\mathbb{N}^+$ and any function $g:\mathcal{S}\times\mathcal{A}\to\mathbb{R}^+$:

$$\mathbb{E}_{\pi^k}[g(s_h,a_h)] = \Theta\left(\mathbb{E}_{\pi^{t_k}}[g(s_h,a_h)]\right).$$

Lemma C.6 (Bounding batched regret ($I_1 + I_3$))**.** Let $\widetilde{r}_k$ be defined in (7) and update the policy as in Algorithm 1. Suppose that Assumption 4.5 holds. Then with probability at least $1 - 2\delta$,

$$\sum_{k=1}^{K} \left[J(\pi^*, \widetilde{r}^k) - J(\pi, \widetilde{r}^k)\right] \leq H \log |\mathcal{A}|/\eta + \eta H^3 K/2$$
$$+ 2HK \cdot \sqrt{8H^2 \log(H \cdot \mathcal{N}_{\mathcal{F}}(\epsilon_{\mathcal{F}})/\delta) + 4\epsilon_{\mathcal{F}} N + \gamma} \cdot O\left(\sqrt{\frac{H}{N} \cdot \frac{H^2 + \gamma}{\gamma} \dim_N(\mathcal{F}_h) \log(1/\delta)}\right).$$

Proof. Suppose that the high-probability events in Lemma C.3 and Lemma C.5 hold.

$$\begin{aligned}
\sum_{k=1}^{K} \left[J(\pi^*, \widetilde{r}^k) - J(\pi, \widetilde{r}^k)\right] &= \sum_{k=1}^{K} \Big(V_{1,\pi^*}^{\widetilde{r}^k}(s_1) - V_1^k(s_1)\Big) + \sum_{k=1}^{K} \Big(V_1^k(s_1) - V_{1,\pi^k}^{\widetilde{r}^k}(s_1)\Big) \\
&\leq \sum_{k=1}^{K} \sum_{h=1}^{H} \mathbb{E}_{s_h \sim \pi^*} \left[\langle Q_h^k(s_h, \cdot), \pi_h(\cdot|s_h) - \pi_h^k(\cdot|s_h)\rangle\right] \\
&\quad + \sum_{k=1}^{K} \sum_{h=1}^{H} \mathbb{E}_{(s_h, a_h) \sim \pi^k} \left[Q_h^k(s_h, a_h) - \widetilde{r}(s_h, a_h) - \mathbb{P}_h V_{h+1}^k(s_h, a_h)\right] \\
&\leq H \log |\mathcal{A}|/\eta + \eta H^3 K/2 + 2HK \cdot \sqrt{8H^2 \log(H \cdot \mathcal{N}_{\mathcal{F}}(\epsilon_{\mathcal{F}})/\delta) + 4\epsilon_{\mathcal{F}} N + \gamma} \\
&\quad \cdot O\left(\sqrt{\frac{H}{N} \cdot \frac{H^2 + \gamma}{\gamma} \dim_N(\mathcal{F}) \log(1/\delta)}\right)
\end{aligned}$$

where the first inequality is obtained by applying the value difference lemma C.1 to both terms and then applying Lemma C.3. □

Lemma C.7 (Upper bound for I_2)**.** If we choose $\eta_{\boldsymbol{\theta}} = O(1/\sqrt{H^2 K})$ in Algorithm 1 and update the reward function as shown in (4.3), then with probability $1 - \delta$,

$$\sum_{k=1}^{K} \left[L(\pi^k, r) - L(\pi^k, r^k)\right] \leq \widetilde{O}\left(\sqrt{H^2 K} + \epsilon_E K\right)$$

Proof. From Lemma D.3, we have for any $r \in \mathcal{R}$,

$$\sum_{k=1}^{K} \left[\widehat{L}(\pi^k, r) - \widehat{L}(\pi^k, r^k)\right] \leq O(1/\eta_{\boldsymbol{\theta}} + \eta_{\boldsymbol{\theta}} H^2 K/2). \tag{C.9}$$

From Lemmas D.1 and D.4, with probability at least $1 - \delta$,

$$\begin{aligned}
&\sum_{k=1}^{K} \left[L(\pi^k, r) - L(\pi^k, r^k)\right] \\
&\leq O(1/\eta_{\boldsymbol{\theta}} + \eta_{\boldsymbol{\theta}} H^2 K/2) + O\big(\sqrt{H^2 K \log(1/\delta)}\big) + O(\epsilon_E K),
\end{aligned} \tag{C.10}$$

from which we can complete the proof by substituting the value of $\eta_{\boldsymbol{\theta}}$ into (C.10). □

Theorem C.8 (Restatement of Theorem 4.7)**.** Suppose Assumptions 4.5, 4.1 and 4.2 hold. if we set $\gamma = H^2$, $\epsilon_{\mathcal{F}} = 1/N$, $\eta = \sqrt{\log |\mathcal{A}|}/H\sqrt{K}$, $m = \lfloor \sqrt{K}/H\sqrt{\log |\mathcal{A}|} \rfloor$, $\eta_{\boldsymbol{\theta}} = O(1/\sqrt{H^2 K})$, and $N = \lceil KH \dim_T(\mathcal{F}) \log \mathcal{N}_{\epsilon_{\mathcal{F}}}(\mathcal{F})/\sqrt{\log |\mathcal{A}|} \rceil$, where $K = \left\lceil \left(\frac{T}{H^2 \dim_T(\mathcal{F}) \log \mathcal{N}_{\epsilon_{\mathcal{F}}}(\mathcal{F})}\right)^{2/3} \right\rceil$, then with probability at least $1 - \delta$, Algorithm 1 yields a regret of

$$\widetilde{O}\left(H^{8/3} \big(\dim_T(\mathcal{F}) \log \mathcal{N}_{\epsilon_{\mathcal{F}}}(\mathcal{F})\big)^{1/3} T^{2/3} + \epsilon_E T\right).$$

Proof for Theorem 4.7. Throughout the proof, we suppose the events in Lemma C.6 and Lemma C.7 hold simultaneously.

From the definition of Regret,

$$\begin{aligned}\text{Regret}(T) &\leq (N/m) \cdot \max_{r \in \mathcal{R}} \sum_{k=1}^{K} \mathbb{E}[\ell(\pi^{t_k}, r)] - \ell(\pi^*, r) \\ &\leq (N/m) \cdot O\left(\max_{r \in \mathcal{R}} \sum_{k=1}^{K} \ell(\pi^k, r) - \ell(\pi^*, r) \right), \end{aligned} \tag{C.11}$$

where the last inequality follows from the definition of t_k.

Then we consider the following decomposition for the regret term,

$$\begin{aligned}\max_{r \in \mathcal{R}} \sum_{k=1}^{K} \ell(\pi^k, r) - \ell(\pi^*, r) \leq & \underbrace{\sum_{k=1}^{K} \left[J(\pi^*, r^k) - J(\pi^k, r^k) \right]}_{I_1} \\ & + \underbrace{\sup_{r \in \mathcal{R}} \sum_{k=1}^{K} \left[L(\pi^k, r) - L(\pi^k, r^k) \right]}_{I_2} + \lambda \underbrace{\sum_{k=1}^{K} \left[\text{Int}(\pi^*; \tau^E) - \text{Int}(\pi^k; \tau^E) \right]}_{I_3}, \end{aligned} \tag{C.12}$$

where $I_1 + I_3$ can be controlled by the classic analysis for optimistic policy optimization, I_2 is the regret of an online learning algorithm for the reward function.

From Lemma C.6,

$$\begin{aligned} I_1 + I_3 &\leq \widetilde{O}(H \log |\mathcal{A}|/\eta + \eta H^3 K/2) + \widetilde{O}\left(H^2 K \sqrt{\frac{H}{N} \log(\mathcal{N}_{\mathcal{F}}(\epsilon_{\mathcal{F}}) \dim_T(\mathcal{F})} \right) \\ &\leq \widetilde{O}\left(H^2 \sqrt{K \log |\mathcal{A}|} \right), \end{aligned} \tag{C.13}$$

where the last inequality holds due to the value of η, N we are choosing.

From Lemma C.7,

$$I_2 \leq \widetilde{O}\left(\sqrt{H^2 K} + \epsilon_E K \right). \tag{C.14}$$

Substituting (C.13) and (C.14) into (C.11),

$$\max_{r \in \mathcal{R}} \sum_{k=1}^{K} \ell(\pi^k, r) - \ell(\pi^*, r) \leq \widetilde{O}\left(H^2 \sqrt{K \log |\mathcal{A}|} + \epsilon_E K \right).$$

After we further substitute the value of hyperparameters into (C.11), we obtain

$$\text{Regret}(T) \leq \widetilde{O}\left(H^{8/3} \big(\dim_T(\mathcal{F}) \log \mathcal{N}_{\epsilon_{\mathcal{F}}}(\mathcal{F}) \big)^{1/3} T^{2/3} + \epsilon_E T \right).$$

□

D Auxiliary Lemmas

Lemma D.1 (Azuma-Hoeffding inequality)**.** Let $\{x_i\}_{i=1}^n$ be a martingale difference sequence with respect to a filtration $\{\mathcal{G}_i\}$ satisfying $|x_i| \leq M$ for some constant M, x_i is $\mathcal{G}_{i+1}$-measurable, $\mathbb{E}[x_i|\mathcal{G}_i] = 0$. Then for any $0 < \delta < 1$, with probability at least $1 - \delta$, we have

$$\sum_{i=1}^{n} x_i \leq M \sqrt{2n \log(1/\delta)}.$$

Lemma D.2 (Self-normalized bound for scalar-valued martingales)**.** Consider random variables $(v_n | n \in \mathbb{N})$ adapted to the filtration $(\mathcal{H}_n : n = 0, 1, ...)$. Let $\{\eta_i\}_{i=1}^{\infty}$ be a sequence of real-valued random variables which is $\mathcal{H}_{i+1}$-measurable and is conditionally σ-sub-Gaussian. Then for an arbitrarily chosen $\lambda > 0$, for any $\delta > 0$, with probability at least $1 - \delta$, it holds that

$$\sum_{i=1}^{n} \epsilon_i v_i \leq \frac{\lambda \sigma^2}{2} \cdot \sum_{i=1}^{n} v_i^2 + \log(1/\delta)/\lambda \qquad \forall n \in \mathbb{N}.$$

Lemma D.3 (Regret bound of online gradient descent, Orabona 2019)**.** Let $V \subseteq \mathbb{R}^d$ a non-empty closed convex set with diameter D, i.e., $\max_{\boldsymbol{x},\boldsymbol{y} \in V} \|\boldsymbol{x} - \boldsymbol{y}\|_2 \leq D$. Let $\ell_1, \cdots, \ell_T$ an arbitrary sequence of convex functions $\ell_t : V \to \mathbb{R}$ differentiable in open sets containing V. Pick any $\boldsymbol{x}_1 \in V$ and assume $\eta_{t+1} \leq \eta_t,\ t = 1, \ldots, T$. Then, $\forall \boldsymbol{u} \in V$, the following regret bound holds

$$\sum_{t=1}^{T} (\ell_t(\boldsymbol{x}_t) - \ell_t(\boldsymbol{u})) \leq \frac{D^2}{2\eta_T} + \sum_{t=1}^{T} \frac{\eta_t}{2} \|\boldsymbol{g}_t\|_2^2 \,.$$

Moreover, if η_t is constant, i.e., $\eta_t = \eta\ \forall t = 1, \cdots, T$, we have

$$\sum_{t=1}^{T} (\ell_t(\boldsymbol{x}_t) - \ell_t(\boldsymbol{u})) \leq \frac{\|\boldsymbol{u} - \boldsymbol{x}_1\|_2^2}{2\eta} + \frac{\eta}{2} \sum_{t=1}^{T} \|\boldsymbol{g}_t\|_2^2 \,.$$

Lemma D.4 (Lemma 9, Liu et al. 2024)**.** There exists an absolute constant $c > 0$ such that for any policy $\pi, \widehat{\pi}$ satisfying $\widehat{\pi}_h(a \mid s) \propto \pi_h(a \mid s) \times \exp(L_h(s, a))$ where $\{L_h(s, a)\}_{h \in [H]}$ is set of functions from $\mathcal{S} \times \mathcal{A}$ to $[-1/H, 1/H]$, we have that for any $\tau_H := (s_1, a_1, \ldots, s_H, a_H) \in (\mathcal{S} \times \mathcal{A})^H$:

$$\mathbb{P}^{\widehat{\pi}}(\tau_H) \leq c \times \mathbb{P}^{\pi}(\tau_H).$$